Dear Editor,

We greatly appreciate the editor’s careful handling of the manuscript and the referees’ valuable comments. We have addressed all comments point by point. Corresponding revisions have been made in the manuscript. A marked-up manuscript version has been provided after response to referees.

Response to referee #1:

We highly appreciate the referee's valuable comments and instructive suggestions. We have addressed each comment as below. Corresponding revisions have been made in the manuscript.

This work reports vertical profiles of absorption during summer 2014 at a semirural area in the North China Plain. Profiles up to 1 km a.g.l. were measured by a single wavelength absorption monitor onboard a tethered balloon. Even though the area where the flights took place is reported as semi rural the measured concentrations are high and comparable to many polluted urban areas, as the authors state in the abstract (p1 l23-24). However in the manuscript no comparison is found between the surrounded areas and the area where the flights took place. Under such high concentrations, a validation in my point of view is required (see also my comment below). In addition, the authors do not report the diurnal and, most important, temporal cycle of absorbing aerosol in that area. The reader is left questioned whether the reported concentrations correspond to the maximum, minimum or average concentrations in that area.

Even though the vertical profile analysis done in this work is, in my point of view, complete and comprehensible with assistive figures, it is not complemented by any discussion on the surrounding area and the particulate temporal variations. I also found disappointing that instead of showing a map of the measurement area, a reference is used instead. The manuscript must be complete by itself.

We thank the referee for the helpful comments. The figure mentioned in the manuscript shows the spatial distribution of average aerosol optical depth (AOD) at 550 nm from the level 2 version of the Moderate Resolution Imaging Spectroradiometer (MODIS) data (Levy and Hsu, 2015) during April 2013 and March 2015 in the NCP (Fig.1 in Ran et al., 2016). Considering that no extra information was given, we did not put this figure in the manuscript. Instead, a description of the sampling site (38°14’N, 115°44’E, miswritten as 38.14°N, 115.44°E there) was present with the cited reference Ran et al. (2016), which has just been published in Atmospheric Environment. However, we agree with the referee that the manuscript should be complete by itself. Thus, an illustration of the AOD distributions in different months of 2014 in the NCP is given in the revised manuscript to provide a direct view of the site and its surroundings. It could also cast some light on the seasonal variation of ambient aerosols in the area where launches of the tethered balloon were carried out, since measurements of absorbing aerosols are unavailable to obtain the temporal variation in that area.

The feature of regional aerosol pollution with clearly defined pollution centers could be recognized from the AOD distributions in different months of the year 2014 (Fig. R1, also as Fig. 1 in the revised manuscript). The level of AOD in Raoyang could well represent regional aerosol conditions in central NCP in July 2014, the month when most of tethered balloon flights took place (Fig. R1c). Moreover, given severe regional aerosol pollution in the NCP, it was understandable that reported BC concentrations in the semirural site of Raoyang were quite high and even comparable to some polluted urban centers in the world.

However, it should be noted that the seasonal cycle of ambient aerosols depends on both the aerosol loading and the relative humidity. As a consequence, the seasonal variation of ambient aerosols obtained from the AOD distributions might not be able to fully represent that of the aerosol loading, not even to mention that of absorbing aerosols. Besides, the diurnal cycle of absorbing aerosols would also be affected by the evolution of the mixing layer and meteorological parameters such as wind speed and direction. Therefore, it is complicated to draw a definite conclusion only from the AOD dataset about to what extent reported BC concentrations represent the spatiotemporal variability in this area.

To gain more confidence in the spatial representativeness of the sampling site, BC emissions (0.25°×0.25°) from four sectors in 2012 in the NCP region were obtained from the multi-resolution emission inventory for China (MEIC, http://www.meicmodel.org) model. Figure R2 (also as Fig. S1 in the supplement) shows the spatial distribution of BC emissions from the sector of industry, power, residential activity and transportation. Centers of intense emissions could be clearly seen, generally coincided with pollution centers in the AOD map. According to the emission inventory of BC, the site of Raoyang could represent the regional situation, also might be influenced by several centers with heavy industry and transportation emissions in the surrounding area.

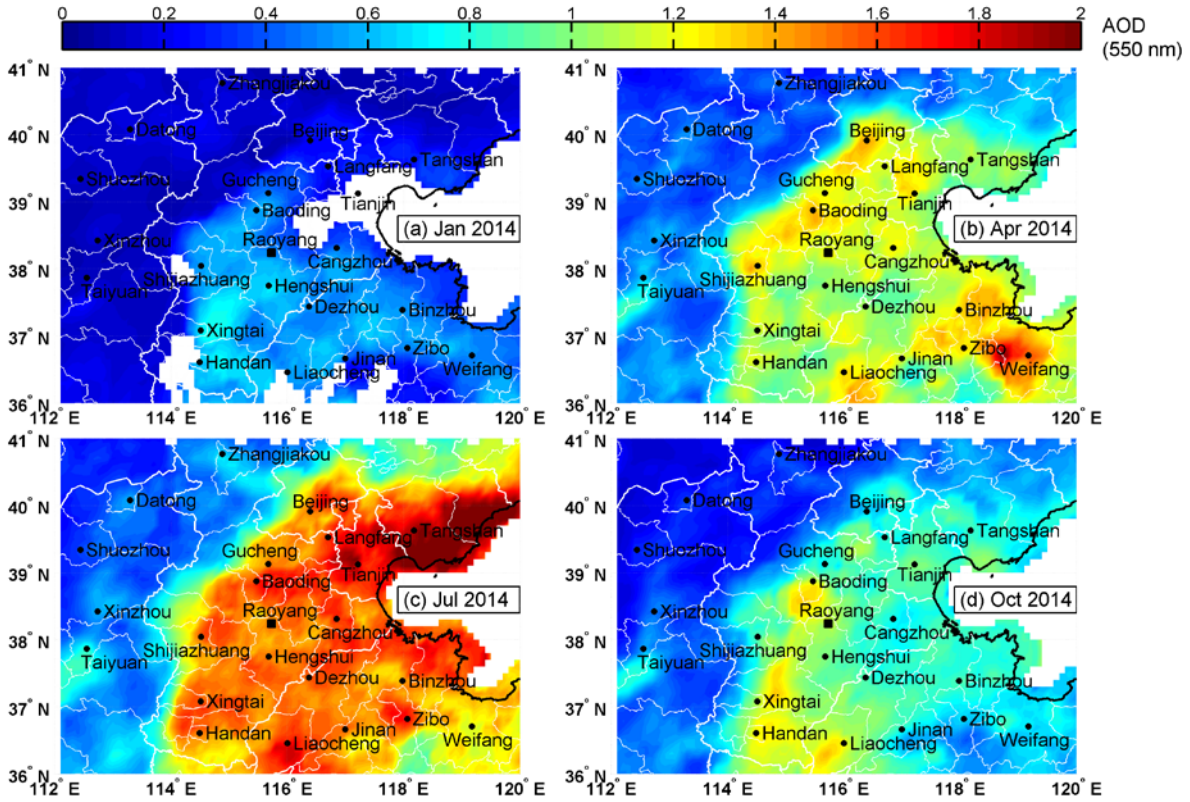

Figure R1. The spatial distribution of averaged MODIS aerosol optical depth (AOD) at 550 nm in (a) January; (b) April; (c) July; (d) October, 2014 in the NCP. The locations of the semirural site Raoyang and major cities are respectively marked by square and dots. Only grids with the fraction of valid data exceeding 30% in the month are shown.

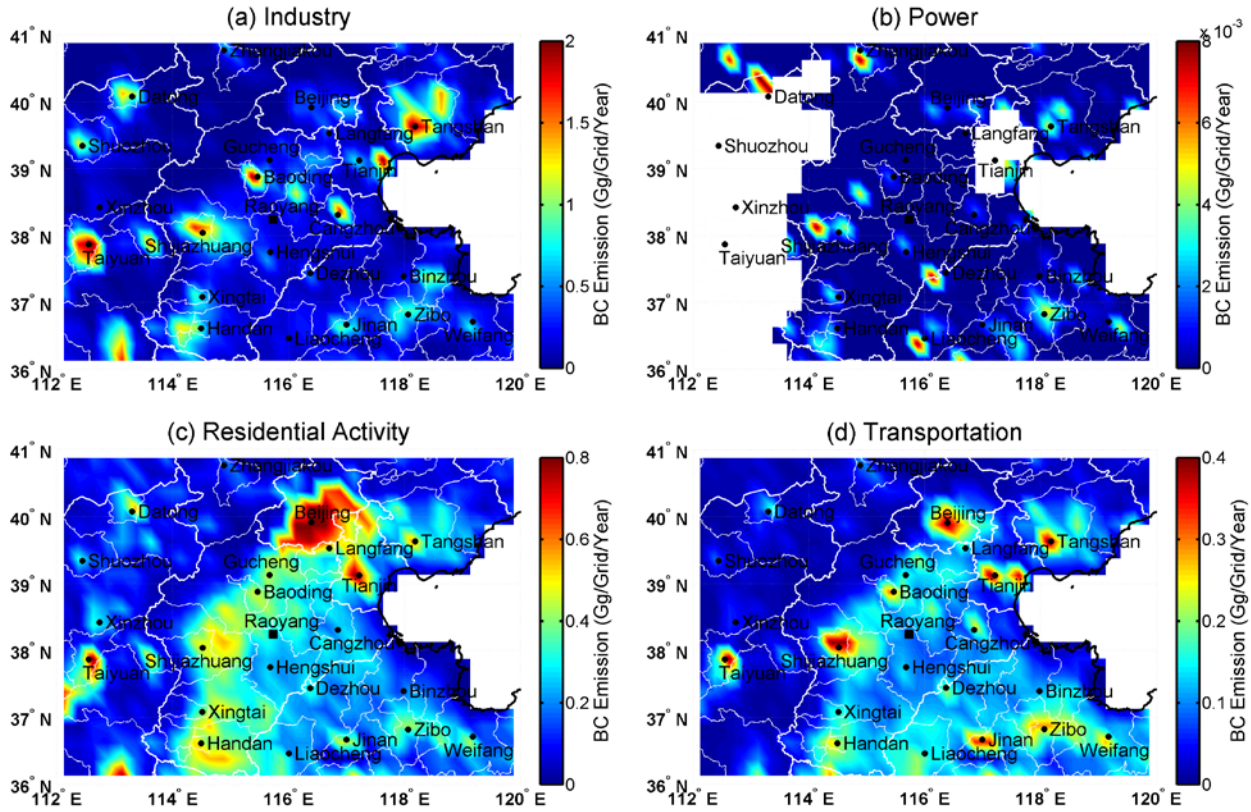

Figure R2. The spatial distribution of BC emissions from the sector of (a) Industry; (b) Power; (c) Residential Activity; (d) Transportation, based upon the emission inventory from the MEIC Model.

Furthermore, seasonal and diurnal variations of surface BC mass concentrations were analyzed on basis of about six-year measurements (from 2006 January to 2012 July with the data completeness of 77.5%) using an aethalometer (Model AE-31, Magee Scientific, USA) with a temporal resolution of 5 min in Gucheng, about 90 km north of Raoyang (Zhang et al., 2015). BC mass concentrations averaged about 9.6±8.4 μg m^{-3} during 2006 and 2012 in Gucheng, with a lower level in summer and spring. The diurnal cycle of BC mass concentrations indicated higher values at night and a low valley in the afternoon. Similar to Raoyang, Gucheng is a semirural site surrounded by city clusters in the NCP (Fig. R1). Measurements at both sites showed a high level of BC that was comparable to many polluted urban areas, which might be surprising but understandable in such a severely polluted region. Also due to the similarity in the AOD level and BC emissions at both sites, BC mass concentrations measured in summer at Raoyang might probably be lower than that in other seasons.

Following above discussions, we have revised the manuscript as:

P3, L11, "The spatial distribution of average aerosol optical depth (AOD) at 550 nm acquired from the level 2 version of the Moderate Resolution Imaging Spectroradiometer (MODIS) data (Levy and Hsu, 2015) is also displayed in Fig. 1. The feature of severe regional aerosol pollution with clearly defined pollution centers could be recognized from the AOD distributions in different months of the year 2014. The level of AOD in Raoyang could well represent regional aerosol conditions in NCP in July 2014, the month when most of tethered balloon flights took place (Fig. 1c). The AOD distributions could also cast some light on the seasonal variation of ambient aerosols in the area where launches of the tethered balloon were carried out, since measurements of absorbing aerosols are unavailable to obtain the temporal variation in that area. However, it should be noted that the seasonal cycle of ambient aerosols depends on both the aerosol loading and the relative humidity. As a consequence, it is complicated to draw a definite conclusion only from the AOD dataset about to what extent reported BC concentrations in this study represent the spatiotemporal variability in the area. A further examination on BC emissions (0.25°×0.25°) from four sectors (industry, power, residential activity, and transportation) in 2012 in the NCP region was performed on basis of emission data generated from the multi-resolution emission inventory for China (MEIC, http://www.meicmodel.org) model. It could also tell from the emission inventory of BC, that aerosol conditions at the site of Raoyang well represents the regional situation, with influences from several nearby emission centers (Fig. S1).

Moreover, it was found that another semirural site Gucheng, about 90 km north of Raoyang, shared a similarity with Raoyang in the AOD level as well as BC emissions. Seasonal and diurnal variations of surface BC mass concentrations in Gucheng were analyzed on basis of about six-year measurements (from 2006 January to 2012 July with the data completeness of 77.5%) using an aethalometer (Model AE-31, Magee Scientific, USA) with a temporal resolution of 5 min (Zhang et al., 2015). BC mass concentrations averaged about 9.6±8.4 μg m^{-3} during 2006 and 2012 in Gucheng, with a lower level in summer and spring. The diurnal cycle of BC mass concentrations indicated higher values at night and a low valley in the afternoon. Thus, it might be expected that BC mass concentrations measured in summer at Raoyang were probably lower than that in other seasons."

Additionally, the authors report a multiple scattering optical enhancement factor C equal to 2.52 using a mass attenuation cross-section equal to 12.5 m^2 g^{-1}. I strongly support enhancing that part, as it holds the greatest interest. The authors should give more details on how the C factor was calculated and provide, as a minimum, a graphical representation of the results. As an example, Ferrero et al. (2011) reports C equal to 2.05 instead. The AE-51 cannot operate on a 24/7 basis. It was never designed to do so. Therefore, the authors should provide more details on how they conducted the comparison.

We totally agree with the referee that we should strengthen the part regarding the calculation of the *C* factor in the manuscript, considering its importance to data processing and subsequent discussions. We also agree with the referee that AE-51 is in principle not designed to be operated around the clock. Continuous comparative measurements using AE-51, AE-31, and MAAP were however carried out, in order to obtain a proper size of the

data for the calculation of the *C* factor in limited time period. A daily check of the flow rate was performed using a Gilibrator-2 Diagnostic Kit (Sensidyne, USA), to ensure the stability of the flow and thus data quality.

The calculation of the *C* factor was based upon concomitant aerosol absorption measurements using AE-51, AE-31 and MAAP for about 1 week in Beijing. The actual wavelength of MAAP is 637 nm instead of the nominal wavelength of 670 nm (Müller et al., 2011), as pointed out by one of the referees for Ran et al. (2016). Accordingly, we have corrected all related results in the revised manuscript.

Three steps were taken to obtain the *C* factor. Firstly, aerosol absorption Angström exponent (α) for the spectrum over the span of 637 and 880 nm was estimated using AE-31 measurements at the channels of 660 and 880 nm. Attenuation coefficients at 660 and 880 nm were corrected to derive absorption coefficients $\sigma_{\text{AE-31,660nm}}$ and $\sigma_{\text{AE-31,880nm}}$. The correction scheme was the same as that in Ran et al. (2016). Then, α was calculated from:

$$\alpha = \frac{\ln(\sigma_{\text{AE-31,660nm}}) - \ln(\sigma_{\text{AE-31,880nm}})}{\ln(880) - \ln(660)}. \quad \text{(R1)}$$

Secondly, $\sigma_{\text{MAAP,880nm}}$ was quantified from $\sigma_{\text{MAAP,637nm}}$ following the spectral dependence of aerosol absorption coefficients in the form of $\lambda^{-\alpha}$:

$$\sigma_{\text{MAAP,880nm}} = \sigma_{\text{MAAP,637nm}} \times (\frac{880}{637})^{-\alpha}. \quad \text{(R2)}$$

Finally, $\sigma_{\text{MAAP,880nm}}$ were taken as real values of absorption coefficients at 880 nm. Reduced major axis regression of attenuation coefficients $\sigma_{\text{AE-51,880nm}}$ (ATN<10) measured by AE-51 and absorption coefficients $\sigma_{\text{MAAP,880nm}}$ calculated from MAAP and AE-31 yielded the *C* factor of 2.98±0.05 with 95% confidence (Fig. R3, also as Fig. 2 in the revised manuscript).

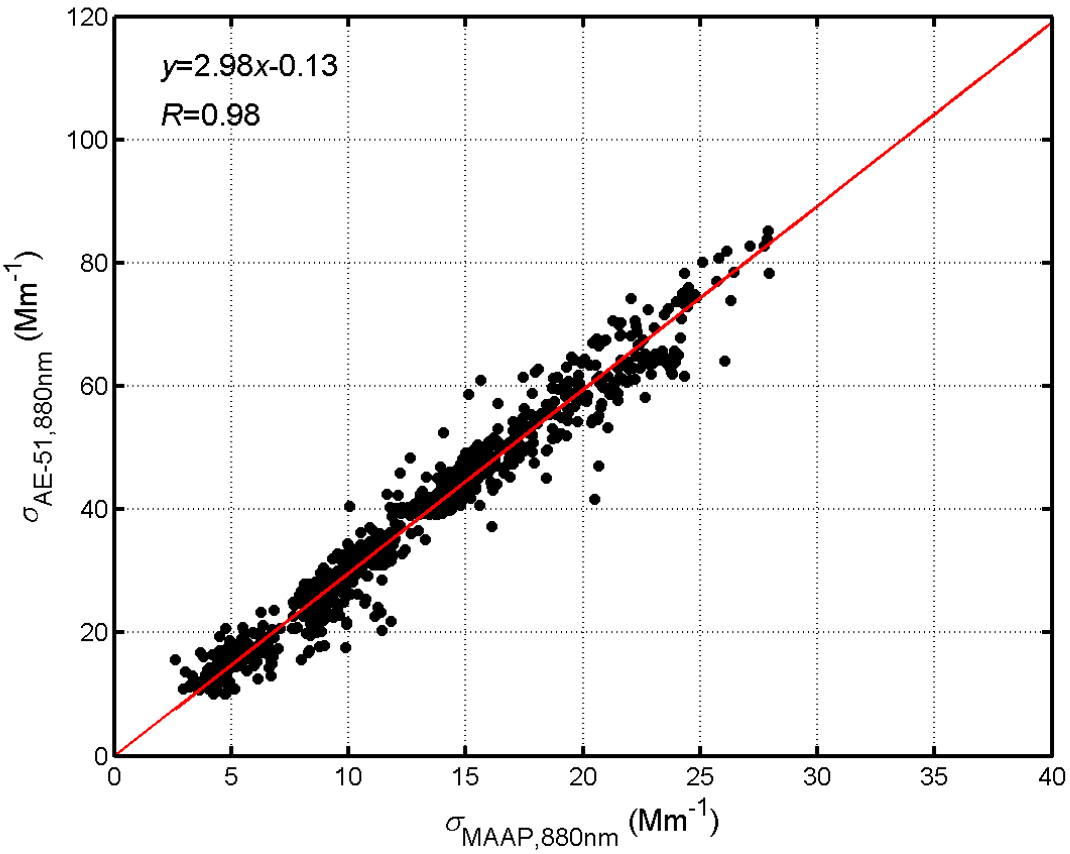

Figure R3. Reduced major axis regression of attenuation coefficients $\sigma_{\text{AE-51,880nm}}$ (ATN<10) measured by AE-51 and absorption coefficients $\sigma_{\text{MAAP,880nm}}$ calculated from concomitant MAAP and AE-31 measurements in the comparative test.

Accordingly, revisions have been made in the manuscript as:

P6, L6, "The *C* factor was derived from a surface comparative test for about 1 week in Beijing among AE-51, a 7-wavelength aethalometer (Model AE-31, Magee Scientific, USA) and a multi-angle absorption photometer (MAAP, Model 5012, Thermo, USA). Continuous operation of AE-51 was carried out in order to obtain a proper size of the dataset in limited time period, despite that AE-51 is in principle not designed to be operated around the clock. A daily check of the flow rate was performed using a Gilibrator-2 Diagnostic Kit (Sensidyne, USA) to ensure the stability of the flow and thus data quality."

P6, L30, "Three steps were taken to obtain the *C* factor. Firstly, aerosol absorption Angström exponent (α) over the spectrum span of 660 and 880 nm was derived from absorption coefficients $\sigma_{\text{AE-31,660nm}}$ and $\sigma_{\text{AE-31,880nm}}$, which were corrected from attenuation coefficients at 660 and 880 nm measured by AE-31. Hence, α was calculated from:

$$\alpha = \frac{\ln(\sigma_{\text{AE-31,660nm}}) - \ln(\sigma_{\text{AE-31,880nm}})}{\ln(880) - \ln(660)}. \quad (2)$$

Secondly, α for the spectrum of 660 and 880 nm was used to represent α over the span of 637 and 880 nm. Therefore, $\sigma_{\text{MAAP,880nm}}$ was quantified from measured $\sigma_{\text{MAAP,637nm}}$ following the spectral dependence of aerosol absorption coefficients in the form of $\lambda^{-\alpha}$:

$$\sigma_{\text{MAAP,880nm}} = \sigma_{\text{MAAP,637nm}} \times \left(\frac{880}{637}\right)^{-\alpha}, \quad (3)$$

Finally, reduced major axis regression of attenuation coefficients $\sigma_{\text{AE-51,880nm}}$ (ATN<10) measured by AE-51 and absorption coefficients $\sigma_{\text{MAAP,880nm}}$ calculated from MAAP and AE-31 yielded the *C* factor of 2.98±0.05 with 95% confidence (Fig. 2)."

On top of that, I recommend the authors to read Hyvarinen et al., (2013, doi:10.5194/amt-6-81-2013). In that work MAAP was reported to underestimate BC concentrations even when the sample was measured onto fresh sample-spots. Even though MAAP and AE51 use different methods to derive BC mass (or absorption) the sampling strategy remains the same; sample is accumulated on a sample spot. Even though the face velocity of AE51 is a factor of 3 lower than that of MAAP, it does not exclude that the effect described in Hyvarinen et al., (2013) does not take place here. The comparison performed here, but discussed too briefly, can shed a light on this. It will also add value to the vertical profiles shown in this work.

We appreciate the referee's valuable suggestion. Hyvärinen et al. (2013) reported an artifact in measuring BC mass concentrations using MAAP, namely, an underestimation after a spot change. This artifact was considered possibly to be associated with erroneous dark counts in the transmitted light photodetector and an instrument internal averaging procedure of the photodetector raw signals. It was stated that this artifact could be observed with a BC mass accumulation rate, as the product of BC mass concentrations and the flow rate of MAAP, larger than 0.04 μg min^{-1}, which corresponds to 3 μg m^{-3} at the flow rate of 1 m^3 h^{-1}. However in this study, no apparent underestimation of BC mass concentrations was found at the beginning of a spot, in comparison with the last several samples collected on the previous spot, even for cases where BC mass concentrations exceeded 8 ug m^{-3}, which stood for an accumulation rate of 0.107 μg min^{-1} with the flow rate of 0.8 m^3 h^{-1} here (Fig. R4, also as Fig. S2 in the supplement). Consequently, no corrections were needed for the MAAP measurements in this study as in Hyvärinen et al. (2013). As for aethalometers, either AE-31 or AE-51, no such effect has been encountered in current experiment and previous studies, also no related literature has been found. Nonetheless, we have added some discussions on this issue in the revised manuscript to leave it open to the community.

P6, L23, "Hyvärinen et al. (2013) reported an artifact of underestimated BC mass concentrations after a spot change and attributed it to yet unconfirmed causes as erroneous dark counts in the transmitted light photodetector and an instrument internal averaging procedure of the photodetector raw signals. It was stated that this artifact

could be observed with a BC mass accumulation rate, as the product of BC mass concentrations and the flow rate of MAAP, larger than 0.04 μg min^{-1}, which corresponds to 3 μg m^{-3} at the flow rate of 1 m^3 h^{-1}. However, no apparent underestimation of BC mass concentrations was found in this study, even for cases where BC mass concentrations exceeded 8 ug m^{-3} (Fig. S2). Consequently, measured $\sigma_{MAAP,637nm}$ without any corrections were used for subsequent calculations and taken as real values."

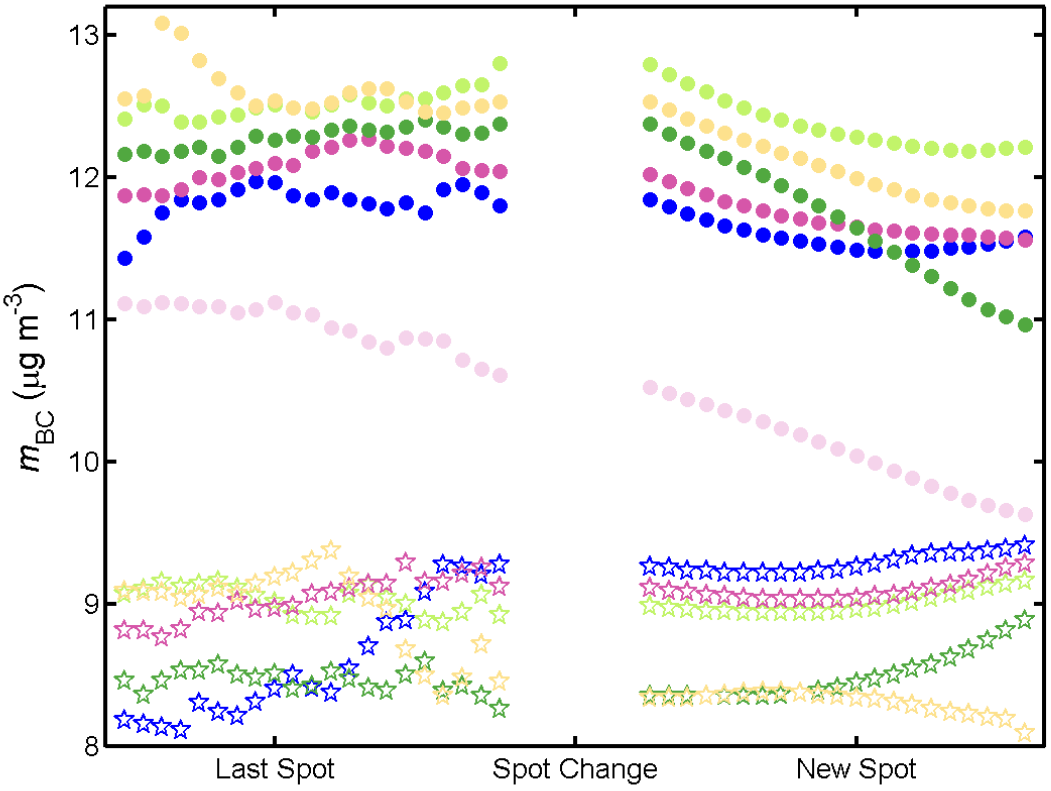

Figure R4. A comparison between measurements using MAAP across filter spot changes for cases where BC mass concentrations exceeded 8 ug m^{-3}. Data points (with a temporal resolution of 1 min) collected before and after a spot change were denoted by the same marker in the same color.

My last remark concerns the smoothing algorithm. I understand that on a single wavelength monitor a smoothing algorithm is primarily used to remove outliers and make measurements more presentable. Under this perspective the authors provide adequate information on the smoothing process. However, multi-wavelength miniature absorption instruments are on the way and a proper smoothing algorithm is essential in calculating the angstrom exponent, as an example. Therefore I strongly encourage the authors to provide a comparison of unsmoothed dataset against those of the proposed algorithm and of Hagler et al. (2011).

We thank the referee for this helpful comment. We proposed in this study a new smoothing algorithm, Fluctuation Minimizing Smoothing (FMS). With properly chosen smoothing window and smoothing count, data fluctuation resulted from the high temporal resolution could be effectively minimized. A comparison was made between unsmoothed data, smoothed data using the FMS approach in this study and the ONA method in Hagler et al. (2011), as well as 20-m averaged data using those two algorithms. Two examples are given below to show that both algorithms could well deal with noises in the signal without introducing artificial features (Fig. R5, also as Fig. 3 in the revised manuscript). However, the FMS method was found to be more capable of reliably removing outliers in some cases (e.g., Fig. R5d-R5f). The comparison indicated that the FMS procedure reduced more fluctuation, meanwhile still preserved reasonable variability of the data.

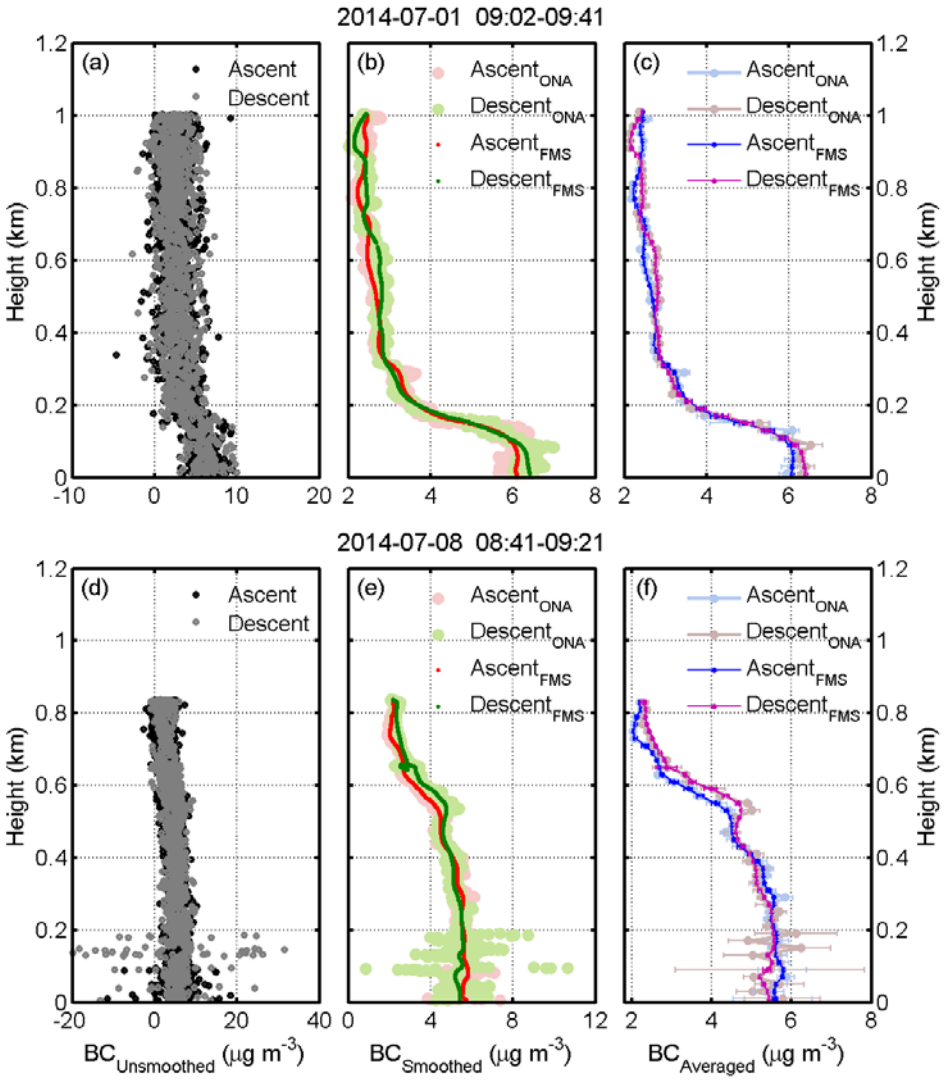

Figure R5. (a) Unsmoothed BC mass concentrations measured with a temporal resolution of 1 s on July 1, 2014 (09:02-09:41 LT). Data points collected from the ascending and descending process are respectively marked in black and grey dots. (b) Smoothed BC mass concentrations using two algorithms. Data points processed by the ONA method are displayed in large pink dots for the ascent and in light green color for the descent. Data points processed by the FMS method are denoted by small red dots for the ascent and green dots for the descent. (c) 20-m averaged profiles based upon smoothed data using two algorithms. Dots indicate 20-m averages, with standard deviations in error bars. Results from the ONA and FMS methods are respectively given in the color of light blue and blue for the ascent, while in the color of light purple and purple for the descent. (d)-(f) Measured and processed BC vertical profiles on July 8, 2014 (08:41-09:21 LT). The caption is the same as that in (a)-(c).

Following the referee's suggestion, we have revised the manuscript as:

P5, L23, "A comparison was made between unsmoothed data, smoothed data using the FMS approach in this study and the ONA method in Hagler et al. (2011), as well as 20-m averaged data using those two algorithms. It was found that both algorithms could properly deal with data fluctuation caused by instrumental noises without introducing artificial features (e.g., Fig. 3a-3c). However, the FMS method seemed to be more capable of reliably removing outliers in some cases (e.g., Fig. 3d-3f). The comparison indicated that the FMS procedure could effectively reduce data fluctuation while still preserve reasonable variability of the profile."

Moreover, we have corrected a mistake in the description of the smoothing algorithm.

P5, L8, "…, where i=1,2,…,N-1,N and j=1,2,…,n-1,n;"

Minor comments p1, L23-25. Please specify which polluted urban areas you are referring to.

We have specified the polluted areas in the revised manuscript as:

P1, L22, "During the field campaign, C_m averaged about 5.16±2.49 μg m^{-3}, with a range of 1.12 to 14.49 μg m^{-3}, comparable with observational results in many polluted urban areas such as Milan in Italy and Shanghai in China."

p3, L5-10. Please add an image of the area, instead of a reference. Currently this work is somewhat incomplete.

We have added a figure as Fig. 1 in the revised manuscript to show the site and its surrounding area, as given in the response to the first comment.

p3, L19. what exactly does that statement means. Can you specify the conditions under which the AE-51 cannot operate. I am a bit surprised as this instrument has been used in drones moving with km h^{-1} speed.

We thank the referee for pointing out the ambiguous statement. Actually, the reason for lack of data is not that AE-51 itself could not operate under strong winds, but that the violent swing of the tethered balloon and the instrument caused poor data quality. As long as the tethered balloon could maintain stable and the instrument kept its posture, valid data could be obtained even under continuous winds if not so strong. However, the randomly varying wind gusts could bring about large artificial variations in measured data. During one launch, the drier prior to the inlet of AE-51 was even torn apart by strong winds. Under such situations, the measurements were considered invalid and the data were discarded. To be clearer, we have revised the manuscript as:

P4, L11, "Lack of data for several ascending or descending processes was primarily caused by discarding invalid data under wind gusts, which led to the violent swing of the tethered balloon and poor data quality."

p5, L9. please provide more details on how the artifacts were addressed. Start by briefly mentioning what artifacts you are referring to. This is not obvious to the reader. The manuscript should be complete.

We have given a more detailed description of the artifacts and the way they were addressed in the revised manuscript as:

P5, L30, "Measured $\sigma_{AE\text{-}51,880nm}$ suffered from systematic biases introduced by the filter-based technique. In order to determine BC absorption coefficients (σ_{BC}) from $\sigma_{AE\text{-}51,880nm}$, corrections were required to tackle with three types of artifacts. The shadowing effect, an artifact that results in gradual artificial reduction in $\sigma_{AE\text{-}51,880nm}$ due to the saturation of the filter with increasing aerosol loading, leads to an underestimation of σ_{BC} and a discontinuity after changing to a new sample spot (Weingartner et al., 2003). Various methods have been developed to address the shadowing effect (Weingartner et al., 2003; Virkkula et al., 2007; Ran et al., 2016). However, this artifact could be neglected in this study, since no ATN exceeded 20 with a new filter for each launch. The other two artifacts cause an overestimation of σ_{BC} by enhancing light attenuation, either due to aerosol scattering or the multiple scattering of filter fibers (Weingartner et al., 2003; Arnott et al., 2005; Schmid et al., 2006; Collaud Coen et al., 2010). A correction factor (C) was needed to correct these two artifacts."

p6, L5-6. how does this affect the measurements. What is the diurnal variation in this area?

The dataset was largely collected in the morning and evening as could be found in Table 1, since a stable condition suitable for launches of the tethered balloon were often encountered then. Around the midday and in the afternoon, surface wind speed usually increased (Fig. R6). It often became very difficult to launch the tethered balloon, due to strong winds and sometimes strong vertical wind shear even not high above the ground.

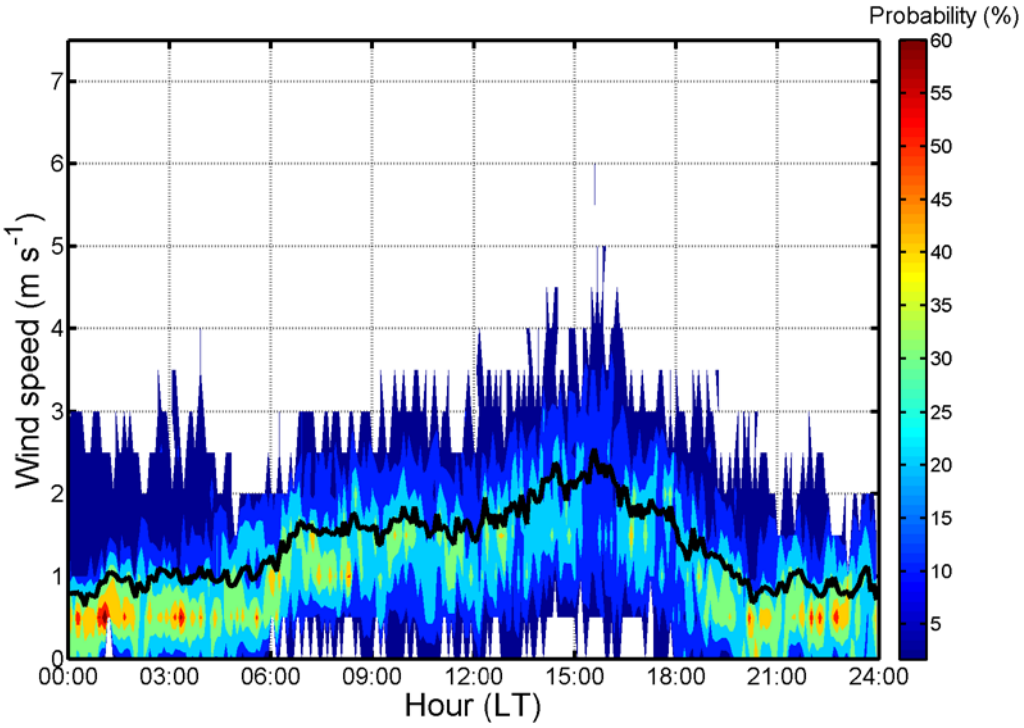

Figure R6. The average diurnal cycle of surface wind speed measured by the automatic weather station at the site on days when tethered balloon flights took place (black line). Color shows the probability of wind speed with an interval of 0.5 m s^{-1} encountered at different time with an interval of 5 min.

p6, L29. I suspect a typo at Larzridis, 2011

Thank you. We have corrected the typo in the revised manuscript.

On page 6 the authors mention two methods from estimating the boundary layer height. Please discuss the differences in PBL height from these two methods.

Following the referee's suggestion, a comparison was made between the mixing height determined from profiles of m_{BC} using the gradient method ($H_{m,BC,gradient}$) and the sigmoid function ($H_{m,BC,sigmoid}$) for typical daytime BC vertical profiles. It was found that results from the two methods generally agreed quite well with each other, with a difference of less than 2 % (Fig. R7, also as Fig. S5 in the supplement). In addition to reliably estimating the mixing height as the gradient method, the sigmoid function could also directly provide parameters including C_{ms}, C_{fs}, and H_e. Therefore, the sigmoid function was applied in the manuscript to obtain all those parameters for typical daytime BC vertical profiles.

Above discussions have been added in the revised manuscript. We have also added Fig. S3 in the supplement (Fig. R8 here) to show the demonstrated well agreement among mixing heights estimated from vertical profiles of m_{BC} using the gradient method ($H_{m,BC,gradient}$) and that of θ ($H_{m,\theta}$) and q ($H_{m,q}$) for the entire dataset.

P8, L21, "The mixing height could be determined by applying the gradient method to the entire dataset (Seibert et al., 2000; Kim, et al., 2007). Generally, the mixing height determined from profiles of m_{BC} ($H_{m,BC,gradient}$) agreed well with that from profiles of θ ($H_{m,\theta}$) and q ($H_{m,q}$) as shown in Fig. S3."

P8, L30, "A comparison was made between $H_{m,BC,gradient}$ and $H_{m,BC,sigmoid}$ for typical daytime BC vertical profiles. Results from the two methods agreed quite well with each other, with a difference of less than 2 % (Fig. S5). In addition to reliably estimating the mixing height as the gradient method, the sigmoid function could also directly determine parameters including C_{ms}, C_{fs}, and H_e. Therefore, the sigmoid function was chosen to obtain all parameters for typical daytime BC profiles."

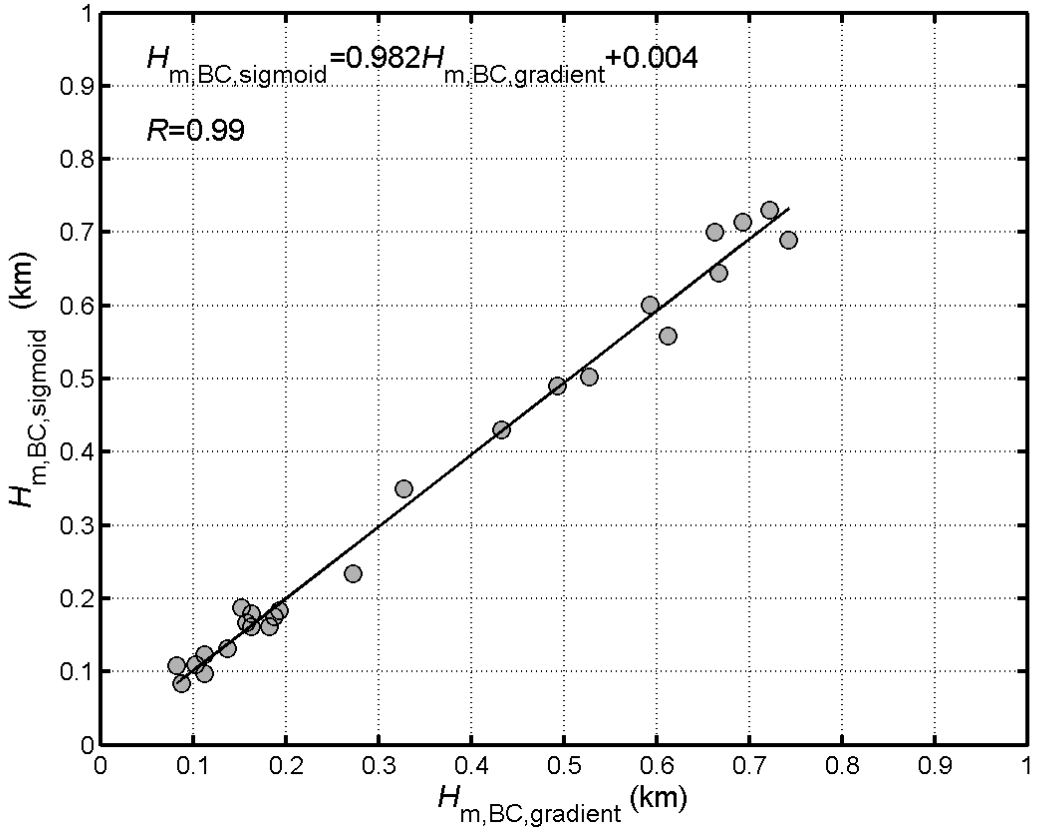

Figure R7. A comparison between mixing heights estimated from vertical profiles of m_{BC} using the gradient method ($H_{m,BC,gradient}$) and the sigmoid function ($H_{m,BC,sigmoid}$) for typical daytime profiles.

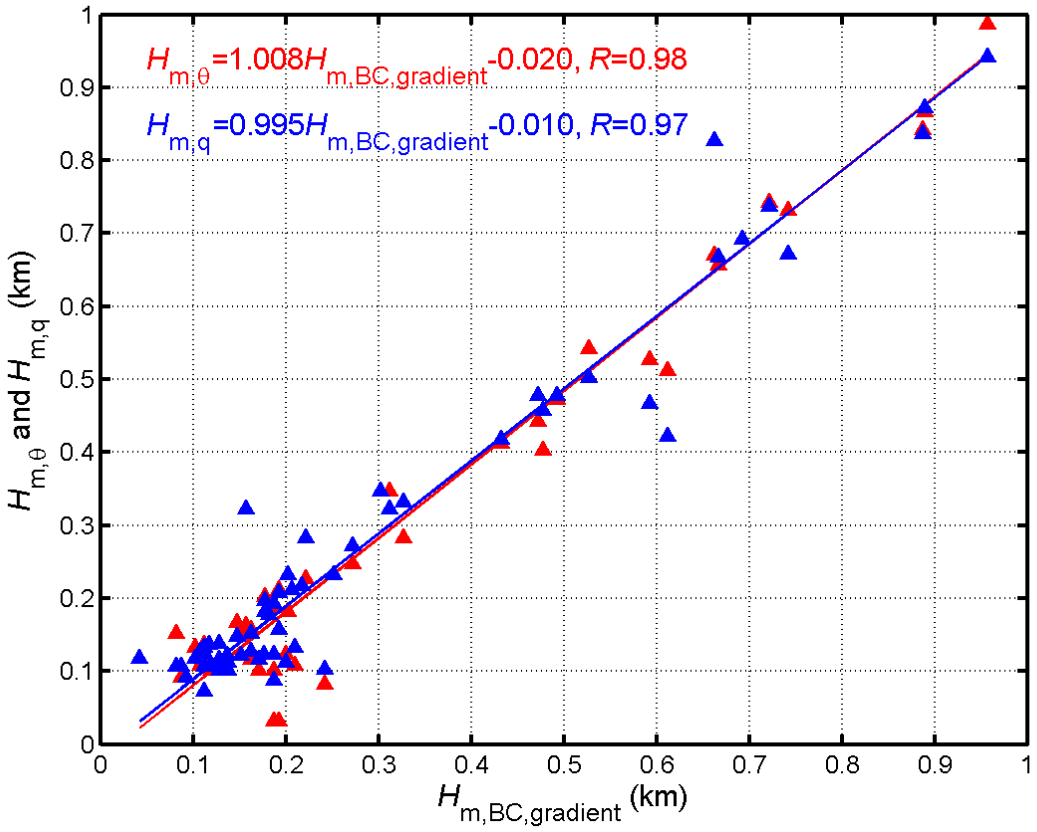

Figure R8. A comparison among mixing heights estimated from vertical profiles of m_{BC} using the gradient method ($H_{m,BC,gradient}$) and that of θ ($H_{m,\theta}$) and q ($H_{m,q}$) for the entire dataset.

p7, L16-17. Were these frequent vertical profiles complemented by ground measurements somewhere close by?

Unfortunately, ground measurements of black carbon mass concentrations are not available.

p8, L1-2. Was there any measurements performed the previous night. What was the result?

There were no measurements carried out the previous night of July 1 due to strong winds. The experiment was designed to collect nighttime vertical profiles, and also to conduct continuous measurements across several days, but the outcome was eventually decided by the weather.

References

Arnott, W. P., Hamasha, K., Moosmuller, H., Sheridan P. J., and Ogren J. A.: Towards aerosol light-absorption measurements with a 7-wavelength aethalometer: evaluation with a photoacoustic instrument and 3-wavelength nephelometer, Aerosol Sci. Tech., 39, 17-29, doi:10.1080/027868290901972, 2005.

Collaud Coen, M., Weingartner, E., Apituley, A., Ceburnis, D., Fierz-Schmidhauser, R., Flentje, H., Henzing, J. S., Jennings, S. G., Moerman, M., Petzold, A., Schmid, O., and Baltensperger, U.: Minimizing light absorption measurement artifacts of the aethalometer: evaluation of five correction algorithms, Atmos. Meas. Tech., 3, 457-474, doi:10.5194/amt-3-457-2010, 2010.

Hagler, G. S. W., Yelverton, T. L. B., Vedantham, R., Hansen, A. D. A. and Turner, J. R.: Post-Processing Method to Reduce Noise while Preserving High Time Resolution in Aethalometer Real-Time Black Carbon Data, Aerosol Air Qual. Res., 11, 539-546, doi:10.4209/aaqr.2011.05.0055, 2011.

Hyvärinen, A. P., Vakkari, V., Laakso, L., Hooda, R. K., Sharma, V. P., Panwar, T. S., Beukes, J. P., van Zyl, P. G., Josipovic, M., Garland, R. M., Andreae, M. O., Pöschl, U., and Petzold, A.: Correction for a measurement artifact of the Multi-Angle Absorption Photometer (MAAP) at high black carbon mass concentration levels, Atmos. Meas. Tech., 6, 81-90, doi:10.5194/amt-6-81-2013, 2013.

Kim, S. W., Yoon, S. C., Won, J. G., and Choi, S. C.: Ground-based remote sensing measurements of aerosol and ozone in an urban area: a case study of mixing height evolution and its effect on ground-level ozone concentrations, Atmos. Environ., 41, 7069-7081, doi:10.1016/j.atmosenv.2007.04.063, 2007.

Levy, R., and Hsu, C.: MODIS Atmosphere L2 Aerosol Product, NASA MODIS Adaptive Processing System, Goddard Space Flight Center, USA, http://dx.doi.org/10.5067/MODIS/MOD04_L2.006, and http://dx.doi.org/10.5067/MODIS/MYD04_L2.006, 2015.

Müller, T., Henzing, J. S., de Leeuw, G., Wiedensohler, A., Alastuey, A., Angelov, H., Bizjak, M., Collaud Coen, M., Engström, J. E., Gruening, C., Hillamo, R., Hoffer, A., Imre, K., Ivanow, P., Jennings, G, Sun, J. Y., Kalivitis, N., Karlsson, H., Komppula, M., Laj, P., Li, S. M., Lunder, C., Marinoni, A., Martins dos Santos, S., Moerman, M., Nowak, A., Ogren, J. A., Petzold, A., Pichon, J. M., Rodriquez, S., Sharma, S., Sheridan, P. J., Teinilä, K., Tuch, T., Viana, M., Virkkula, A., Weingartner, E., Wilhelm, R., and Wang, Y. Q.: Characterization and intercomparison of aerosol absorption photometers: result of two intercomparison workshops, Atmos. Meas. Tech., 4, 245-268, doi:10.5194/amt-4-245-2011, 2011.

Ran, L., Deng, Z. Z., Wang, P. C., and Xia, X. A.: Black carbon and wavelength-dependent aerosol absorption in the North China Plain based on two-year aethalometer measurements, Atmos. Environ., 142, 132-144, doi:10.1016/j.atmosenv.2016.07.014, 2016.

Schmid, O., Artaxo, P., Arnott,W. P., Chand, D., Gatti, L. V., Frank, G. P., Hoffer, A., Schnaiter, M., and Andreae, M. O.: Spectral light absorption by ambient aerosols influenced by biomass burning in the Amazon Basin. I: comparison and field calibration of absorption measurement techniques, Atmos. Chem. Phys., 6, 3443-3462, doi:10.5194/acp-6-3443-2006, 2006.

Seibert, P., Beyrich, F., Gryning, S. E., Joffre, S., Rasmussen, A., and Tercier, P.: Review and intercomparison of operational methods for the determination of the mixing height, Atmos. Environ., 34. 1001-1027, doi:10.1016/S1352-2310(99)00349-0, 2000.

Virkkula, A., Mäkelä, T., Hillamo, R., Yli-Tuomi, T., Hirsikko, A., Hämeri, K., and Koponen, I. K.: A simple procedure for correcting loading effects of aethalometer data, J. Air Waste Manage. Assoc, 57, 1214-1222, doi:10.3155/1047-3289.57.10.1214, 2007.

Weingartner, E., Saathoff, H., Schnaiter, M., Streit, N., Bitnar, B., and Baltensperger, U.: Absorption of light by soot particles: determination of the absorption coefficient by means of aethalometers, J. Aerosol Sci., 34, 1445-1463,

doi:10.1016/S0021-8502(03)00359-8, 2003.

Zhang, X., Tang, J., Wu, Y. F., Wu, J., Yan, P., and Zhang, R. J.: Variations of black carbon aerosol observed in Beijing and surrounding area during 2006-2012, China Powder Sci. Tech., 21, 24-35, doi:10.13732/j.issn.1008-5548.2015.04.006, 2015.

Response to referee #2:

We highly appreciate the referee's valuable comments and instructive suggestions. We have addressed each comment as below and corresponding revisions have been made in the manuscript.

This paper report results of vertical profiles of black carbon aerosol collected in the North China Plain. The topic and the reported measurements are very important as vertical profile data of BC a globally scarce if compared with the high amount of ground-based observation. Thus the topic of this paper is of fundamental importance. It is suitable to be published on ACP after the authors raised the following points.

MAIN POINTS: Abstract (page 1 lines 12-20): the development of the mixing layer is qualitatively described. Moreover it is reported that the mixing layer usually developed from 0.2 km up to 1 km (i.e. sunny days) and followed by a "collapse" during the evening. In a such situation a residual layer usually forms above the NBL making the concentration measured above the mixing layer not representative of a clean free troposphere. Please discuss also the possible importance of the residual layer formation on your measurements along the entire manuscript.

We thank the referee for the valuable suggestion. We agree with the referee that the existence of a residual layer would make measured BC mass concentrations (m_{BC}) above the mixing layer not representative of a clean free troposphere. As stated in the manuscript, average m_{BC} in free troposphere could reach 2~3 μg m^{-3} under polluted conditions, otherwise usually well below 1 μg m^{-3} under clean conditions. The case study of vertical profiles measured on July 1 (Fig. 6) showed a polluted layer with a thickness of 0.3 km in the morning, possibly a residual layer formed the day before. The level of m_{BC} above the polluted layer was also as high as ~2 μg m^{-3}. The case study of vertical profiles measured on July 8 (also in Fig. 6) showed how vertical profiles of m_{BC} evolved with the development of the planetary boundary layer (PBL). A relatively high level of m_{BC} was found above the NBL where the remnant of the daytime mixing layer after its collapse might be traced. However, analysis regarding the impact of the residual layer formed in the previous evening on measurements on the next day is difficult to carry out without continuous measurements from the previous day. Also the characteristics of the residual layer should be affected by the advection. The role of the residual layer in affecting the evolution of the PBL still stays controversial, though it has been consented that BC could heat the PBL and intensify atmospheric stability. Ding et al. (2016) demonstrated the importance of the "dome effect" of BC in the PBL especially the upper PBL, suppressing the PBL height and enhancing haze pollution within a lower PBL. However, Zhang et al. (2012) indicated a limited warming effect of BC in an elevated aerosol layer, and also limited induced increase in the strength of atmospheric inversion.

Corresponding discussions in the revised manuscript include:

P10, L8, "This might imply the existence of a polluted residual layer above the stable surface layer formed after the sunset in previous evening, yet unable to be further discussed without continuous measurements from the day before. Also the characteristics of m_{BC} in FT should be affected by the advection."

P10, L17, "Sometimes, a residual layer with a relatively high level of m_{BC} (>2 μg m^{-3}) could be formed above the NBL where the remnant of the daytime mixing layer might be traced after its collapse (e.g., profiles on July 8). This would undoubtedly have an impact on measured m_{BC} above the mixing layer on the next day, leading to a polluted background in FT (e.g., in the morning of July 1 and 8). The role of the residual layer in affecting the evolution of the PBL still stays controversial, though it has been consented that BC could heat the PBL and intensify atmospheric stability. Ding et al. (2016) demonstrated the importance of the "dome effect" of BC in the PBL especially the upper PBL, suppressing the PBL height and enhancing haze pollution within a lower PBL. Whereas in Zhang et al. (2012), a limited warming effect of BC in an elevated aerosol layer and limited induced increase in the strength of atmospheric inversion were indicated."

Section 2.2.1: the developed smoothing algorithm appears very promising. However, a deeper discussion here is called for. Especially it is necessary to compare the smoothing results with that can be obtained by the ONA (Hagler et al. (2011)) application. I strongly suggest to introduce a new picture to show the effect

of the two data treatment on the raw collected BC data along vertical profiles. The reason for a such request comes from the fact that the Hagler at al. algorithm is based on the physical behavior of the measured ATN in the Aethalometer, while the new smoothing algorithm reported in this paper appear only statistically based and somehow affected by the operator (i.e. "(6) Repeat step (1)-(5) for m times to obtain acceptable smoothed data"). Concerning the last point in brackets: have you defined a criteria for the "acceptable smoothed data"? How much is the threshold? How much is the loss in terms of vertical resolution of the data after the smoothing? I think the smoothing algorithm should be also discussed more quantitatively than did until now.

We agree with the referee that a comparison between processed data using the two smoothing algorithms, Fluctuation Minimizing Smoothing (FMS) method proposed in this study and the ONA method in Hagler et al. (2011), should be made to show the similarity and differences in effects of the two approaches on unsmoothed data. As found in the two cases displayed in Fig. R1 (also as Fig. 3 in the revised manuscript), generally, both algorithms properly treated data fluctuation and largely improved the presented data. However, the FMS procedure seemed to be more capable of reliably reducing data fluctuation without losing details on the variability of vertical profiles (Fig. R1d-R1f).

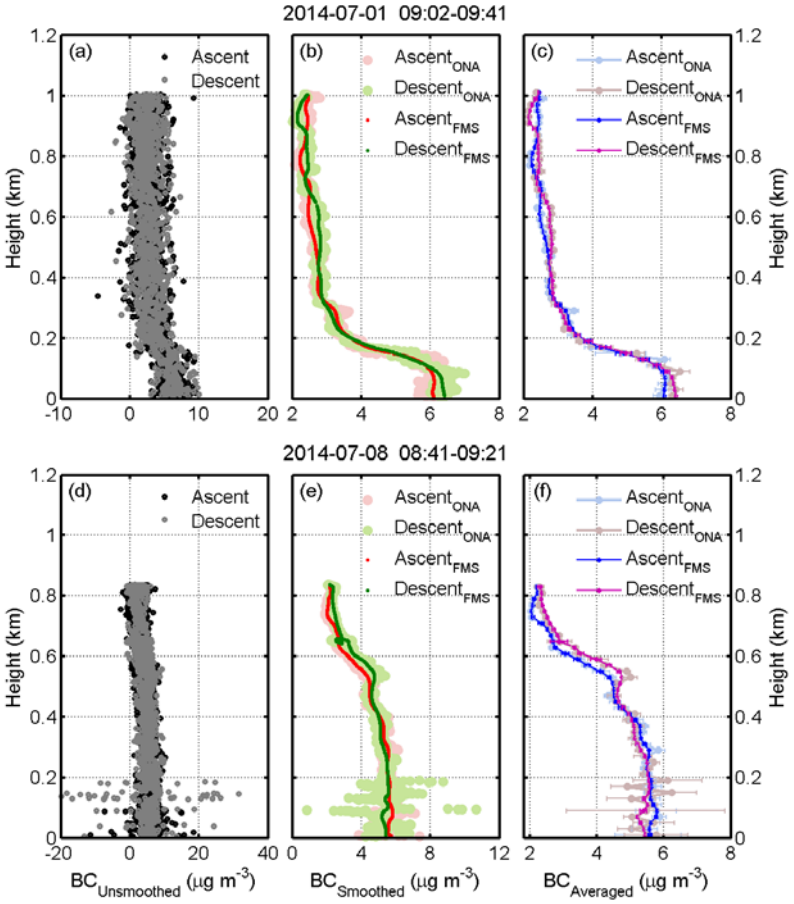

Figure R1. (a) Unsmoothed BC mass concentrations measured with a temporal resolution of 1 s on July 1, 2014 (09:02-09:41 LT). Data points collected from the ascending and descending process are respectively marked in black and grey dots. (b) Smoothed BC mass concentrations using two algorithms. Data points processed by the ONA method are displayed in large pink dots for the ascent and in light green color for the descent. Data points processed by the FMS method are denoted by small red dots for the ascent and green dots for the descent. (c) 20-m averaged profiles based upon smoothed data using two algorithms. Dots indicate 20-m averages, with standard deviations in error bars. Results from the ONA and FMS methods are respectively given in the color of light blue and blue for the ascent, while in the color of light purple and purple for the descent. (d)-(f) Measured and processed BC vertical profiles on July 8, 2014 (08:41-09:21 LT). The caption is the same as that in (a)-(c).

The FMS method was devised to smooth the highly temporally resolved data (1 s) from AE-51. Similar to the ONA method (Hagler et al., 2011), the FMS approach is also principally based upon the physical behavior of measured ATN. Usually, ATN is supposed to increase with time. However, reported ATN might largely fluctuate due to limited sampling on the filter and instrumental noises such as that from the light source, the detector, electronics, the flow rate and unstable posture. Despite that BC values determined from fluctuated ATN might drastically vary, large positive/negative BC pairs would always be found and counterbalance each other within a few seconds. Therefore, the FMS method minimizes data fluctuation by finding pairs of BC values that differ largely with each other within a few seconds and making a compromise of them. The smoothing window *n* used to search for pairs and the smoothing count used to repeat the smoothing were empirically chosen. Normally, data fluctuation is already compensated within 5 s, according to what has been observed in data processing.

To address the loss of the vertical resolution of processed data using the FMS method, the contribution from neighboring data points to the weighted average of each target point was calculated. In the FMS procedure, each data point was averaged within a range of 2*n* data points, where *n* is the smoothing window. The average process was repeated by *m* times, where *m* is the smoothing count. With *n* to be 5 and *m* to be 1 or 5, average weight function for each profile was calculated and the result was similar among profiles. When *m* was set to be 1, the average of the target point was mostly contributed from neighboring data points within about 11 seconds, according to a weight of 80%. This consequently led to a vertical resolution of about 22 m for the ascent and 11 m for the descent after smoothing. Similarly, the vertical resolution was about 50~60 m for the ascent and 25~30 m for the descent when *m* was set to be 5. Figure R2 presents average weight function for two cases as given in Fig. R1. Different choices of the smoothing count gave a similar pattern of vertical profiles, but with some differences in details. To achieve a better smoothing for further calculations, the smoothing count was chosen to be 5 in this work.

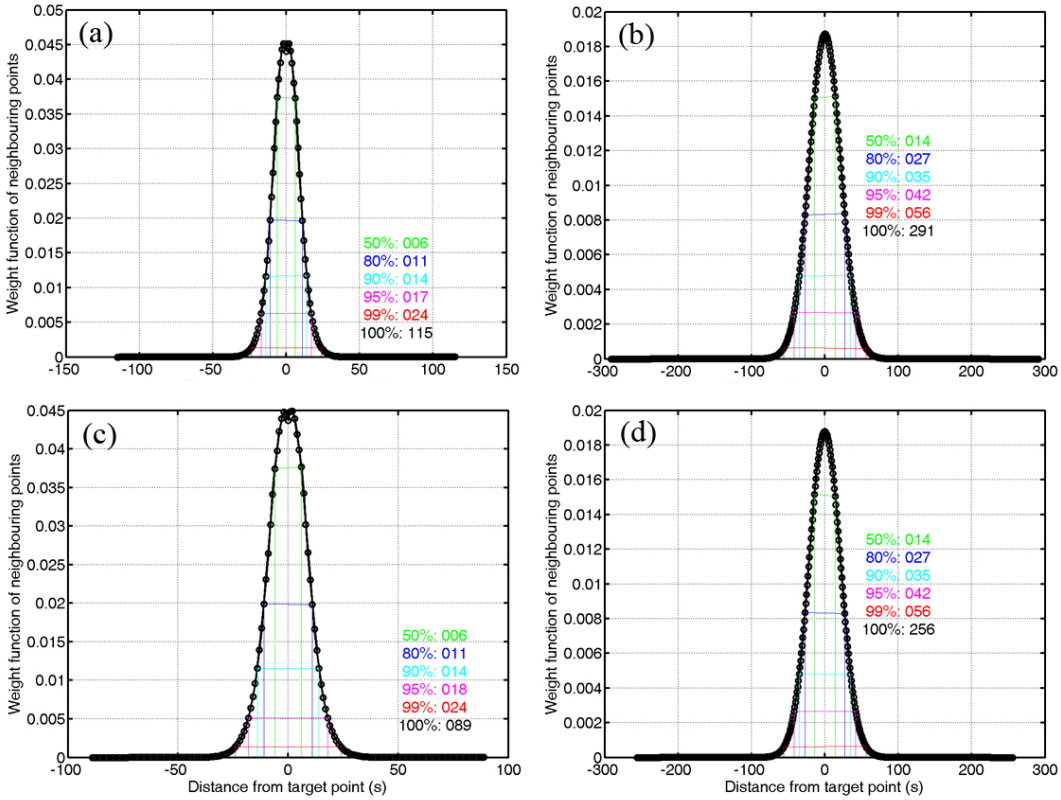

Figure R2 Average weight function of neighboring data points to show their contribution to the weighted average of each target point for the case on July 1, 2014 (09:02-09:41 LT) with the smoothing window *n* to be 5, (a) the smoothing count *m* was set to be 1; (b) *m* was set to be 5. Similar to the first case, average weight function for the case on July 8, 2014 (08:41-09:21 LT), (c) the smoothing count *m* was set to be 1; (d) *m* was set to be 5.

According to above discussions, we have revised the manuscript as:

P4, L30, "In this study, data dispersion due to high temporal resolution was treated by a new smoothing algorithm, Fluctuation Minimizing Smoothing (FMS). Similar to the ONA method, the FMS approach is also principally based upon the physical behavior of measured ATN. Despite that BC values determined from fluctuated ATN might drastically vary, large positive/negative pairs of BC values would always be found and counterbalance each other within a few seconds. Therefore, the FMS approach was devised to find pairs of BC values that differ largely with each other within a few seconds and make a compromise."

P5, L15, "The smoothing window *n* and the smoothing count *m* were empirically chosen during the calculation. It should be kept in mind that using improper large *n* or *m* might wipe off some natural variations, although it will always give a smoother result. *n* should be set to no more than 5, given that data fluctuation is normally already compensated within 5 s. With *n* to be 5 and *m* to be 1, the average of the target point was mostly contributed from neighboring data points within about 11 seconds, according to a weight of 80%. This consequently led to a vertical resolution of about 22 m for the ascent and 11 m for the descent after smoothing. Similarly, the vertical resolution was about 50~60 m for the ascent and 25~30 m for the descent when *m* was set to be 5. Different choices of *m* gave a similar pattern of vertical profiles, but with some differences in details. In this study, *m* was set to be 5 to achieve a better smoothing for further calculations, though this caused a loss of the vertical resolution more than twice as large as that when just smoothing once. A comparison was made between unsmoothed data, smoothed data using the FMS approach in this study and the ONA method in Hagler et al. (2011), as well as 20-m averaged data using those two algorithms. It was found that both algorithms could properly deal with data fluctuation caused by instrumental noises without introducing artificial features (e.g., Fig. 3a-3c). However, the FMS method seemed to be more capable of reliably removing outliers in some cases (e.g., Fig. 3d-3f). The comparison indicated that the FMS procedure could effectively reduce data fluctuation while still preserve reasonable variability of the profile."

Moreover, we have corrected a mistake in the description of the smoothing algorithm.

P5, L8, "…, where i=1,2,…,N-1,N and j=1,2,…,n-1,n;"

Section 2.2.2, page 5, line 8: "Details of the correction scheme developed for tackling with artifacts of AE-31 were described in Ran et al. (2016)". Note that Ran et al. (2016) is just a submitted paper. In the reference list the journal to which Ran et al. paper was submitted is missing. Please add it. Moreover, as the AE31 data could significantly change in function of the chosen correction function it is necessary to resume here at least the main points of the correction scheme adopted in Ran et al. as the paper is not yet available to the scientific community. With respect to this, depending on the chosen correction scheme (i.e. C factors for each wavelength of the AE31), the obtained angstrom exponent should change introducing an error on the retrieved $\sigma_{MAAP,880nm}$. A quantitative assessment of the variability of $\sigma_{MAAP,880nm}$ depending on the chosen correction scheme for the AE31 is called for. Moreover, I strongly recommend an analysis of the error propagation of $\sigma_{MAAP,880nm}$ on the obtained C for the AE51. As a matter of fact the C factor of 2.52 is reported here without any statistical treatment of its uncertainty. Finally, no reference was made to the C value of 2.05±0.03 for the AE51 reported in Ferrero et al. (2011a). It should very interesting to discuss the difference on the two C values in terms of the chemical composition of the aerosol in the NCP with respect to the Europe.

We thank the referee for the helpful and instructive comments. We agree with the referee that more details should be given on the correction scheme adopted in Ran et al. (2016), which has just been published in Atmospheric Environment.

Briefly, the correction scheme used to deal with instrumental artifacts of AE-31 was a combination of the

modified Virkkula method (Virkkula et al., 2007) to treat the shadowing effect and the Schmid method (Schmid et al., 2006) to treat filter multiple scattering and aerosol scattering effects. The modified Virkkula method assumed a linear relationship between BC mass concentrations and time across the filter change, particularly, a quadratic relationship for special cases where ambient BC experienced a peak-shaped variation, instead of the assumption of constant BC mass concentrations in Virkkula et al. (2007). Following procedures in the Schmid method, the wavelength-dependent correction factor (C_λ) could be derived. As the referee stated, the choice of the correction scheme for AE-31 measurements might introduce uncertainties to absorption Angström exponent (α), and thereby pass them to $\sigma_{MAAP,880nm}$ that were calculated from α and absorption coefficients measured at 637 nm ($\sigma_{MAAP,637nm}$) by MAAP. Using a constant C factor for AE-31 as also often used in some studies (e.g., Weingartner et al., 2003; Sandradewi et al., 2008) instead of the wavelength-dependent C_λ results in an underestimation of α over the 660-880 nm spectrum by about 19.5%. This consequently leads to an overestimation of $\sigma_{MAAP,880nm}$ and the C factor for AE-51 by about 9.6% and 8.4%, respectively.

Another important thing to mention is that the actual wavelength of MAAP is 637 nm instead of the nominal wavelength of 670 nm (Müller et al., 2011), as pointed out by one of the referees for Ran et al. (2016). We have accordingly corrected all related results in the revised manuscript. Subsequently, attenuation coefficients $\sigma_{AE\text{-}51,880nm}$ (ATN<10) measured by AE-51 and calculated $\sigma_{MAAP,880nm}$ were employed to yield the C factor using reduced major axis regression (Fig. R3, also as Fig. 2 in the revised manuscript). The C factor was 2.98±0.05 with 95% confidence, quite different from a value of 2.05±0.03 in Ferrero et al. (2011a). Possible explanations on such a difference in the C factor might be found in aerosol chemical compositions in the NCP region and the Po Valley basin. Besides, the C factor in Ferrero et al. (2011a) was obtained from Mie calculations, and thus was subject to uncertainties resulting from assumptions such as BC size distributions, BC mixing state and particle morphology. Also the C factor derived from methods in this study bears some uncertainties as mentioned above.

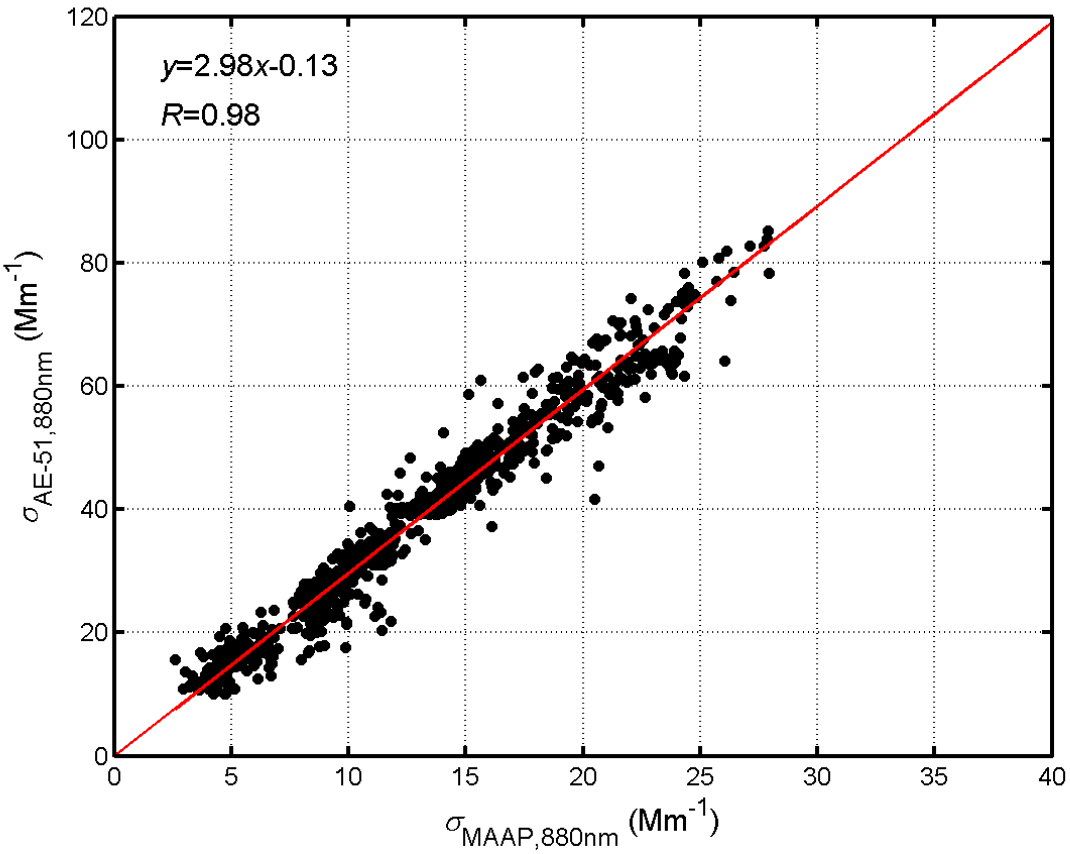

Figure R3. Reduced major axis regression of attenuation coefficients $\sigma_{AE\text{-}51,880nm}$ (ATN<10) measured by AE-51 and absorption coefficients $\sigma_{MAAP,880nm}$ calculated from concomitant MAAP and AE-31 measurements in the comparative test.

Accordingly, revisions have been made in the manuscript as:

P6, L11, "AE-31 suffered instrumental artifacts in the same way as AE-51. Details of the correction scheme developed for tackling with AE-31 artifacts were described in Ran et al. (2016). Briefly, the correction scheme combined the modified Virkkula method (Virkkula et al., 2007) to treat the shadowing effect and the Schmid method (Schmid et al., 2006) to treat filter multiple scattering and aerosol scattering effects. The modified Virkkula method assumed a linear relationship of BC mass concentrations and time across the filter change, particularly, a quadratic relationship for special cases where ambient BC experienced a peak-shaped variation, instead of constant BC mass concentrations as in Virkkula et al. (2007). The wavelength-dependent correction factor (C_λ) could be obtained following procedures in Schmid et al. (2006). The temporal resolution of AE-31 during the comparative test was 2 min."

P6, L30, "Three steps were taken to obtain the *C* factor. Firstly, aerosol absorption Angström exponent (α) over the spectrum span of 660 and 880 nm was derived from absorption coefficients $\sigma_{\text{AE-31,660nm}}$ and $\sigma_{\text{AE-31,880nm}}$, which were corrected from attenuation coefficients at 660 and 880 nm measured by AE-31. Hence, α was calculated from:

$$\alpha = \frac{\ln(\sigma_{\text{AE-31,660nm}}) - \ln(\sigma_{\text{AE-31,880nm}})}{\ln(880) - \ln(660)}. \quad (2)$$

Secondly, α for the spectrum of 660 and 880 nm was used to represent α over the span of 637 and 880 nm. Therefore, $\sigma_{\text{MAAP,880nm}}$ was quantified from measured $\sigma_{\text{MAAP,637nm}}$ following the spectral dependence of aerosol absorption coefficients in the form of $\lambda^{-\alpha}$:

$$\sigma_{\text{MAAP,880nm}} = \sigma_{\text{MAAP,637nm}} \times \left(\frac{880}{637}\right)^{-\alpha} , \quad (3)$$

Finally, reduced major axis regression of attenuation coefficients $\sigma_{\text{AE-51,880nm}}$ (ATN<10) measured by AE-51 and absorption coefficients $\sigma_{\text{MAAP,880nm}}$ calculated from MAAP and AE-31 yielded the *C* factor of 2.98±0.05 with 95% confidence (Fig. 2). It was noted that the *C* factor for AE-51 was reported as 2.05±0.03 with 95% confidence in Ferrero et al. (2011a). Possible explanations on such a difference in the *C* factor might be found in aerosol chemical compositions in the NCP region and the Po Valley basin. Besides, the *C* factor in Ferrero et al. (2011a) was obtained from Mie calculations, and thus was subject to uncertainties resulting from assumptions such as BC size distributions, BC mixing state and particle morphology. In addition, the choice of the correction scheme for AE-31 measurements in this study might introduce uncertainties to α and thereby $\sigma_{\text{MAAP,880nm}}$. Using a constant *C* factor for AE-31 as also often used in some studies (e.g., Weingartner et al., 2003; Sandradewi et al., 2008) instead of the wavelength-dependent C_λ results in an underestimation of α over the 660-880 nm spectrum by about 19.5%. This consequently leads to an overestimation of $\sigma_{\text{MAAP,880nm}}$ and the *C* factor for AE-51 by about 9.6% and 8.4%, respectively."

Page 5, lines 12-13: "Measured $\sigma_{\text{AE-51,880nm}}$ (ATN<10) and calculated $\sigma_{\text{MAAP,880nm}}$ were linearly fitted with a correlation coefficient of 0.96 in a significant level (P<0.001), yielding a C value of 2.52": Please add the picture of this correlation.

We have added a figure as Fig. 2 in the revised manuscript to show this correlation. The figure is given in the response to the last comment.

Page 6, line 13, equation 6: "H_{m} was calculated from a sigmoid function that could well characterize typical daytime profile of m_{BC}:". From this sentence it appears that H_{m} was calculated using equation 6. However, equation 6 requires as input both the mixing layer and the entrainment layer. This point is not clearly defined and needs to be specified. I also suggest to add a graphical example of the mixing layer determination using the sigmoid function. Finally a question: as you have both the potential temperature and wind profiles at disposal, have you ever thought to analyse the mixing layer also using the Richardson

number approach?

We thank the referee for pointing out the interpretation that might have caused confusion. We have added an illustration to show the fitting of BC profiles using the sigmoid function (Fig. R4, also as Fig. S4 in the supplement). We have clarified this point in the revised manuscript as:

P8, L24, "On the other hand, typical daytime profiles of m_{BC} could be well characterized by the sigmoid function:

$$m_{BC} = C_{ms} - \frac{C_{ms} - C_{fs}}{e^{-(h - H_{m,BC,sigmoid})/H_e} + 1} \quad (6)$$

where C_{ms} and C_{fs} are respectively characteristic m_{BC} within the ML and in free troposphere (FT), $H_{m,BC,sigmoid}$ is the mixing height derived from BC vertical profiles using the sigmoid function, H_e represents the thickness of the EL, h is the height at which each 20-m averaged m_{BC} is obtained. The parameters C_{ms}, C_{fs}, $H_{m,BC,sigmoid}$ and H_e could be directly determined by fitting measured m_{BC} at each height h using Eq. (6) as shown by the example (Fig. S4). A comparison was made between $H_{m,BC,gradient}$ and $H_{m,BC,sigmoid}$ for typical daytime BC vertical profiles. Results from the two methods agreed quite well with each other, with a difference of less than 2 % (Fig. S5). In addition to reliably estimating the mixing height as the gradient method, the sigmoid function could also directly determine parameters including C_{ms}, C_{fs}, and H_e. Therefore, the sigmoid function was chosen to obtain all parameters for typical daytime BC profiles."

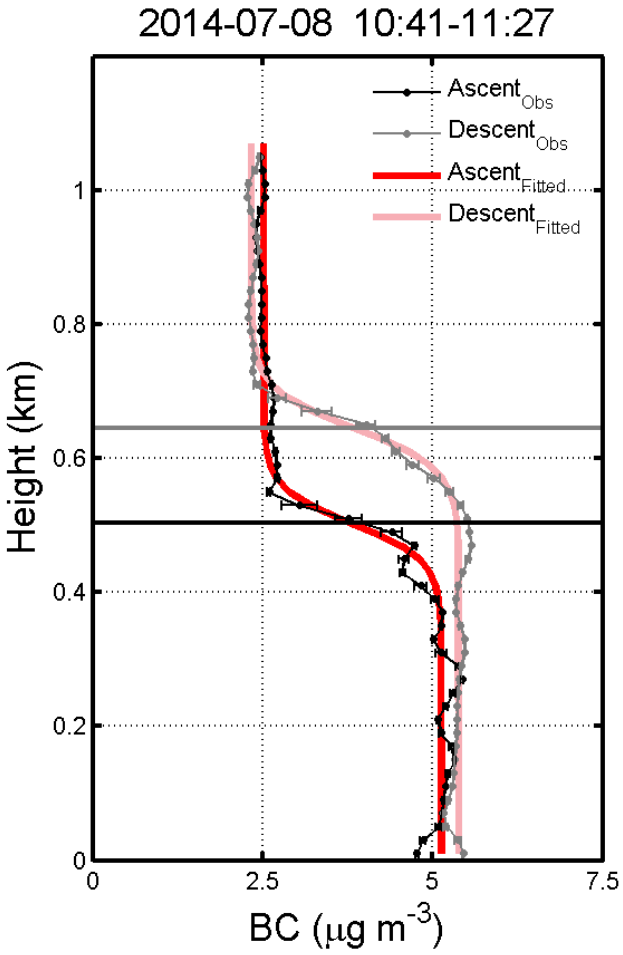

Figure R4. An example of fitting BC vertical profiles using the sigmoid function. Measurements were conducted on July 8, 2014 (10:41-11:27 LT).

Finally, we followed the referee's suggestion and employed the Richardson number approach to determine the mixing height (Vogelezang and Holtslag, 1996; Seibert et al., 2000). Equation (R1) was used to calculate the Richardson number $Ri_b(h)$ for each 5-m layer at the midpoint h, where $\theta_v(h)$ is the virtual potential temperature calculated from potential temperature and the mixing ratio of water vapor, θ_{v1} is the average virtual potential

temperature for the 5-10 m layer, $U(h)$ and $V(h)$ are wind components computed from wind speed and direction, g is the gravity of earth. The mixing height was determined as the height where $Ri_b(h)$ exceeded the classic critical value of 0.25 (Seibert et al., 2000).

$$Ri_b(h) = \frac{gh}{\theta_{v1}} \frac{\theta_{v1}(h) - \theta_{v1}}{U(h)^2 + V(h)^2} \quad \text{(R1)}$$

Figure R5 shows a satisfactory agreement among mixing heights estimated from vertical profiles of θ ($H_{m,\theta}$) and q ($H_{m,q}$) using the gradient method and from the Richardson number approach ($H_{m,RN}$). However, uncertainties in the determination of mixing heights using the Richardson number approach might arise from the accuracy of temperature and wind profiles, the choice of the equation and the critical value. Moreover, the height of the nocturnal boundary layer was poorly determined and corresponding results have been removed in Fig. R5. Therefore, a combination of the sigmoid approach and the gradient method was applied to estimate mixing heights for the entire dataset.

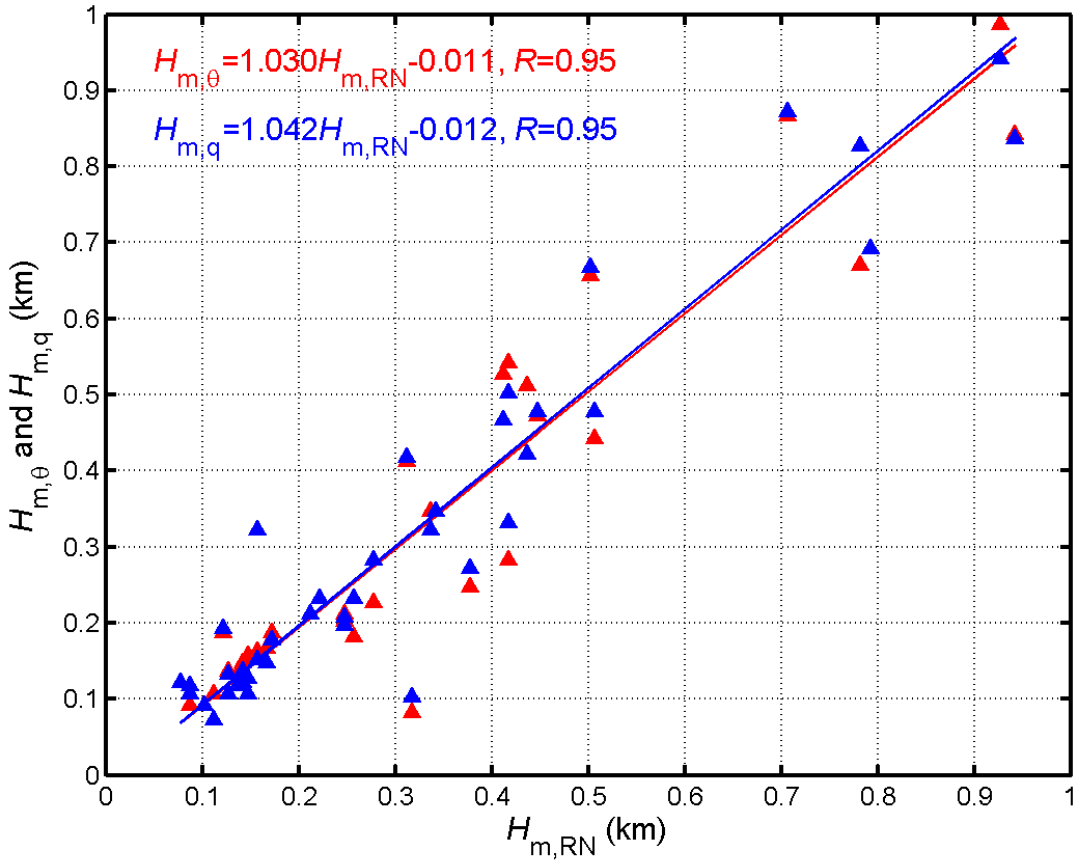

Figure R5. A comparison among mixing heights estimated from vertical profiles of θ ($H_{m,\theta}$) and q ($H_{m,q}$) using the gradient method, and that from the Richardson number approach ($H_{m,RN}$).

MINOR POINTS: Page 7, lines 3-4: "the normalized height (H_{Nor}), which was calculated from h/H_m-1". In Ferrero et al. (2014) this analysis is explained. Add this reference at the end of the sentence.

We thank the referee for this helpful comment. We have revised the manuscript as:

P9, L17, "Statistically, vertical profiles of BC were categorized into two types, according to their shapes along the normalized height (H_{Nor}), which was calculated from h/H_m-1 (Ferrero et al., 2014)."

Figure 2b: at H_{Nor}=0 BC data are characterized by free troposphere concentration levels. I was a bit surprised about it. I expected that around H_{Nor}=0 there was at least the end of the exponential decrease of concentration starting from ground values. Could you comment it?

We thank the referee for pointing this out. As expected, the height around H_{Nor}=0 is indeed the end of the exponential decrease of m_{BC} starting from the ground value for individual profile. Figure 2b (as Fig. 5b in the revised manuscript) displays each vertical profile of m_{BC} in the evening (grey lines). Above the NBL (H_{Nor}>0), no apparent decrease in m_{BC} was found for individual profile. However, the level of m_{BC} above H_{Nor}=0 differed largely in different cases, representing clean or relatively polluted conditions in FT. Hence, the average profile presents an artificial feature of a decrease in m_{BC} even above H_{Nor}=0. To clarify the confusing feature of the average profile, we have revised the manuscript as:

P9, L27, "For each BC profile (grey lines in Fig. 5b), m_{BC} nearly exponentially declined with H_{Nor}, as a result of weakened turbulence and vertical dispersion."

Page 3, lines 24-25 and equation 1: "to estimate aerosol absorption coefficients at the wavelength of 880 nm following"… Please note that $\sigma_{AE\text{-}51,880nm}$ is the attenuation coefficient and not the absorption coefficient as reported in many papers (i.e. starting from Weingartner et al. (2003)). Please correct the paper for this point.

We thank the referee for this valuable comment. We have corrected the manuscript as:

P4, L18, "…simultaneously detected to obtain attenuation coefficients at the wavelength of 880 nm ($\sigma_{AE\text{-}51,880nm}$)…"

References

Ding, A. J., Huang, X., Nie, W., Sun, N. J., Kerminen, V. M., Petäjä, T., Su, H., Cheng, Y. F., Yang, X. Q., Wang, M. H., Chi, X. G., Wang, J. P., Virkkula, A., Guo, W. D., Yuan, J., Wang, S. Y., Zhang, R. J. Zhang, Wu, Y. F., Song, Y. Song, Zhu, T., Zilitinkevich, S., Kulmala, M., and Fu, C. B.: Enhanced haze pollution by black carbon in megacities in China, Geophys. Res. Lett., 43, 2873-2879, doi:10.1002/2016GL067745, 2016.

Ferrero, L., Mocnik, G., Ferrini, B. S., Perrone, M. G., Sangiorgi, G., and Bolzacchini, E.: Vertical profiles of aerosol absorption coefficient from micro-aethalometer data and Mie calculation over Milan, Sci. Total Environ., 40, 2824-2837, doi:10.1016/j.scitotenv.2011.04.022, 2011a.

Ferrero, L., Castelli, M., Ferrini, B. S., Moscatelli, M., Perrone, M. G., Sangiorgi, G., D'Angelo, L., Rovelli, G., Moroni, B., Scardazza, F., Mocnik, G., Bolzacchini, E., Petitta, M., and Cappelletti, D.: Impact of black carbon aerosol over Italian basin valleys: high-resolution measurements along vertical profiles, radiative forcing and heating rate, Atmos. Chem. Phys., 14, 9641-9664, doi:10.5194/acp-14-9641-2014, 2014.

Hagler, G. S. W., Yelverton, T. L. B., Vedantham, R., Hansen, A. D. A. and Turner, J. R.: Post-Processing Method to Reduce Noise while Preserving High Time Resolution in Aethalometer Real-Time Black Carbon Data, Aerosol Air Qual. Res., 11, 539-546, doi:10.4209/aaqr.2011.05.0055, 2011.

Müller, T., Henzing, J. S., de Leeuw, G., Wiedensohler, A., Alastuey, A., Angelov, H., Bizjak, M., Collaud Coen, M., Engström, J. E., Gruening, C., Hillamo, R., Hoffer, A., Imre, K., Ivanow, P., Jennings, G, Sun, J. Y., Kalivitis, N., Karlsson, H., Komppula, M., Laj, P., Li, S. M., Lunder, C., Marinoni, A., Martins dos Santos, S., Moerman, M., Nowak, A., Ogren, J. A., Petzold, A., Pichon, J. M., Rodriquez, S., Sharma, S., Sheridan, P. J., Teinilä, K., Tuch, T., Viana, M., Virkkula, A., Weingartner, E., Wilhelm, R., and Wang, Y. Q.: Characterization and intercomparison of aerosol absorption photometers: result of two intercomparison workshops, Atmos. Meas. Tech., 4, 245-268, doi:10.5194/amt-4-245-2011, 2011.

Ran, L., Deng, Z. Z., Wang, P. C., and Xia, X. A.: Black carbon and wavelength-dependent aerosol absorption in the North China Plain based on two-year aethalometer measurements, Atmos. Environ., 142, 132-144, doi:10.1016/j.atmosenv.2016.07.014, 2016.

Sandradewi, J., Prevot, A. S. H., Weingartner, E., Schmidhauser, R., Gysel, M., and Baltensperger, U.: A study of wood burning and traffic aerosols in an Alpine valley using a multi-wavelength aethalometer, Atmos. Environ., 42, 101-112, doi:10.1016/j.atmosenv.2007.09.034, 2008 .

Schmid, O., Artaxo, P., Arnott, W. P., Chand, D., Gatti, L.V., Frank, G. P., Hoffer, A., Schnaiter, M., an Andreae, M. O.: Spectral light absorption by ambient aerosols influenced by biomass burning in the Amazon Basin. I: comparison and field calibration of absorption measurement techniques, Atmos. Chem. Phys., 6, 3443-3462, doi:10.5194/acp-6-3443-2006, 2006.

Seibert, P., Beyrich, F., Gryning, S. E., Joffre, S., Rasmussen, A., and Tercier, P.: Review and intercomparison of operational methods for the determination of the mixing height, Atmos. Environ., 34. 1001-1027, doi:10.1016/S1352-2310(99)00349-0, 2000.

Virkkula, A., Mäkelä, T., Hillamo, R., Yli-Tuomi, T., Hirsikko, A., Hämeri, K., and Koponen, I. K.: A simple procedure for correcting loading effects of aethalometer data, J. Air & Waste Manage. Assoc., 57, 1214-1222, doi:10.3155/1047-3289.57.10.1214 , 2007.

Vogelezang, D. H. P., and Holtslag, A. A. M.: Evolution and model impacts of alternative boundary layer formulations, Boundary-Layer Meteorol., 81, 245-269, doi:10.1007/BF02430331, 1996.

Weingartner, E., Saathoff, H., Schnaiter, M., Streit, N., Bitnar, B., and Baltensperger, U.: Absorption of light by soot particles: determination of the absorption coefficient by means of aethalometers, J. Aerosol Sci., 34, 1445-1463, doi:10.1016/S0021-8502(03)00359-8, 2003.

Zhang, D. Z., Chen, B., Yamada, M., Niu, H. Y., Wang, B., Iwasaka, Y., and Shi, G. Y.: Elevated soot layer in polluted urban atmosphere: a case study in Beijing, J. Meteorol. Soc. Japan, 90, 361-375, doi:10.2151/jmsj.2012-302, 2012.

Vertical profiles of black carbon measured by a micro-aethalometer in summer in the North China Plain

L. Ran[1], Z. Z. Deng[1], X. B. Xu[2], P. Yan[3], W. L. Lin[3], Y. Wang[2], P. Tian[4], P. C. Wang[1], W. L. Pan[1], D. R. Lu[1]

[1]Key Laboratory of Middle Atmosphere and Global Environment Observation, Institute of Atmospheric Physics, Chinese Academy of Sciences, Beijing, 100029, China
[2]Key Laboratory for Atmospheric Chemistry, Institute of Atmospheric Composition, Chinese Academy of Meteorological Sciences, Beijing, 100081, China
[3]Meteorological Observation Center, China Meteorological Administration, Beijing, 100081, China
[4]Beijing Weather Modification Office, Beijing, 100089, China

Correspondence to: L. Ran (shirleyrl@mail.iap.ac.cn) and Z. Z. Deng (dengzz@mail.iap.ac.cn)

Abstract. Black carbon (BC) is a dominant absorber in visible spectrum and a potent factor in climatic effects. Vertical profiles of BC were measured using a micro-aethalometer attached to a tethered balloon during the Vertical Observations of trace Gases and Aerosols (VOGA) field campaign, in summer 2014 at a semirural site in the North China Plain (NCP). The diurnal cycle of BC vertical distributions following the evolution of the mixing layer was investigated for the first time in the NCP region. Statistical parameters including identified mixing height (H_m) and average BC mass concentrations within the mixing layer (C_m) and in free troposphere (C_f) were obtained for a selected dataset of 67 vertical profiles. H_m was usually lower than 0.2 km in the early morning and rapidly rose thereafter due to strengthened turbulence. The maximum height of the ML was reached in late afternoon. The top of a full developed ML exceeded 1 km on sunny days in summer, while stayed much lower on cloudy days. The sunset triggered the collapse of the ML and a stable nocturnal boundary layer (NBL) gradually formed. Accordingly, the highest level C_m was found in the early morning and the lowest in the afternoon. In the daytime, BC almost uniformly distributed within the ML and significantly decreased above the ML. During the field campaign, C_m averaged about 5.16±2.49 μg m^{-3}, with a range of 1.12 to 14.49 μg m^{-3}, comparable with observational results in many polluted urban areas such as Milan in Italy and Shanghai in China. As evening approached, BC gradually built up near the surface and exponentially declined with height. In contrast to the large variability found both in H_m and C_m, C_f stayed relatively unaffected through the day. C_f was less than 10% of the ground level under clean conditions, while amounted to half of the ground level in some polluted cases. In-situ measurements of BC vertical profiles would hopefully have an important implication for accurately estimating direct radiative forcing by BC and improving the retrieval of aerosol optical properties by remote sensing in this region.

删除的内容: BC

1 Introduction

Black carbon (BC), produced from incomplete combustion processes, is a strongly absorbing constituent of atmospheric aerosols (Moosmüller et al., 2009; Bond et al., 2013). As a major absorber in the visible spectrum, BC heats the atmosphere and largely counterbalances cooling effects of scattering aerosols on climate (Jacobson, 2001; Ramanathan et al., 2005; Stier et al., 2007). Another reason for BC to be publicly concerned is that inhaled BC poses a huge threat to human health (Janssen et al., 2012; Nichols, 2013).

Despite the significance of evaluating radiative forcing by BC, large uncertainties arise from limitations of current knowledge on emissions, distributions and physical properties of BC (Andreae, 2001; Streets, et al., 2001; Bond et al., 2006; IPCC, 2013). One critical aspect pertinent to climate response of BC is a high sensitivity of BC radiative impact to its vertical distributions (Zarzycki and Bond, 2010; Ban-Weiss et al., 2012; Samset et al., 2013). The importance of BC vertical distributions to the evolution of planetary boundary layer (PBL) and cloud properties has also been demonstrated by previous studies (Yu et al., 2002; Ramanathan and Carmichael, 2008; Ferrero et al., 2014). Nevertheless, vertical profiles of BC or aerosol absorption have only been scarcely measured in a few field campaigns (Safai et al., 2012 and references therein; Ryerson et al., 2013). Available information on BC vertical distributions are particularly limited in China (Zhang et al., 2012; Li et al., 2015; Zhao et al., 2015), issuing a challenge to reliably estimate regional climatic effects of BC under severe air pollution due to rapid economic growth and urbanization in this region (Menon et al., 2002; Liao and Shang, 2015 and references therein).

Platforms normally utilized to perform BC profiling are tethered balloons, aircrafts and unmanned aerial vehicles. BC vertical profiles obtained from in-situ measurements using tethered balloons are highly vertically resolved, revealing details within about 1 km above the ground, especially in the thin surface layer that is vital for human beings and where various sources are located (Ferrero et al., 2011a, Babu et al., 2011a; Li et al., 2015). Comparatively, aircrafts (Tripathi et al., 2005, 2007; Metcalf et al., 2012; Zhao et al., 2015) and unmanned aerial vehicles (Corrigan et al., 2008; Höpner et al., 2016) are more expensive, although they have advantages of reaching higher altitudes and for aircrafts more onboard instruments in the size and weight unable to be carried by tethered balloons and unmanned aerial vehicles. Fast flight speeds of these two platforms also compromise their spatial resolutions. In addition, high altitude balloon was employed to measure BC vertical profiles at high altitudes in free troposphere, e. g., two BC polluted layers found at about 4.5 km and 8 km altitudes were reported by Babu et al. (2011b). Indirect methods such as recently proposed Lidar remote sensing might be able to conduct continuous measurements (Miffre et al., 2015), they are however less accurate than in-situ measurements.

To advance understanding in impacts of atmospheric components including trace gases and aerosols on atmospheric environment and climate, an intensive field campaign, Vertical Observations of trace Gases and Aerosols (VOGA), was carried out in summer 2014 at a semirural site in the North China Plain (NCP), one of the most overcrowded and polluted regions in the world (Shao et al., 2006; Xu et al., 2011; Ma et al., 2011; Chen et al., 2012). A tethered balloon system equipped with instruments was employed for high vertical resolution measurements within 1 km above the ground. In this

删除的内容: -

study, we present results from in-situ measurements of BC vertical profiles using a lightweight (about 280 g) and small-sized (117 mm×66 mm×38 mm) micro-aethalometer (microAeth® Model AE-51, Magee Scientific, USA). The diurnal cycle of BC vertical distributions was explored for the first time in the NCP region.

2 Experiment

2.1 The site

The VOGA 2014 field campaign was carried out in the period from June 21 to July 14 at a semirural site Raoyang (38°14'N, 115°44'E, 20 m a.s.l.), about 50 km north of the city of Hengshui in the central NCP (Fig. 1). The county of Raoyang, in which the site is located, is less industrialized and relies mainly on agriculture, but surrounded by a cluster of industrial and populated cities within a distance of 100 km, and respectively about 190 km and 160 km southwest of the twin megacities of Beijing and Tianjin.

The spatial distribution of average aerosol optical depth (AOD) at 550 nm acquired from the level 2 version of the Moderate Resolution Imaging Spectroradiometer (MODIS) data (Levy and Hsu, 2015) is also displayed in Fig. 1. The feature of severe regional aerosol pollution with clearly defined pollution centers could be recognized from the AOD distributions in different months of the year 2014. The level of AOD in Raoyang could well represent regional aerosol conditions in NCP in July 2014, the month when most of tethered balloon flights took place (Fig. 1c). The AOD distributions could also cast some light on the seasonal variation of ambient aerosols in the area where launches of the tethered balloon were carried out, since measurements of absorbing aerosols are unavailable to obtain the temporal variation in that area. However, it should be noted that the seasonal cycle of ambient aerosols depends on both the aerosol loading and the relative humidity. As a consequence, it is complicated to draw a definite conclusion only from the AOD dataset about to what extent reported BC concentrations in this study represent the spatiotemporal variability in the area. A further examination on BC emissions (0.25°×0.25°) from four sectors (industry, power, residential activity, and transportation) in 2012 in the NCP region was performed on basis of emission data generated from the multi-resolution emission inventory for China (MEIC, http://www.meicmodel.org) model. It could also tell from the emission inventory of BC, that aerosol conditions at the site of Raoyang well represents the regional situation, with influences from several nearby emission centers (Fig. S1).

Moreover, it was found that another semirural site Gucheng, about 90 km north of Raoyang, shared a similarity with Raoyang in the AOD level as well as BC emissions. Seasonal and diurnal variations of surface BC mass concentrations in Gucheng were analyzed on basis of about six-year measurements (from 2006 January to 2012 July with the data completeness of 77.5%) using an aethalometer (Model AE-31, Magee Scientific, USA) with a temporal resolution of 5 min (Zhang et al., 2015). BC mass concentrations averaged about 9.6±8.4 μg m^{-3} during 2006 and 2012 in Gucheng, with a lower level in summer and spring. The diurnal cycle of BC mass concentrations indicated higher values at night and a low valley in

删除的内容: 38.14°N, 115.44°E
删除的内容: as shown in
删除的内容: in Ran et al. (2016

the afternoon. Thus, it might be expected that BC mass concentrations measured in summer at Raoyang were probably lower than that in other seasons.

2.2 Instruments

A micro-aethalometer to measure aerosol absorption at 880 nm and a radiosonde to measure meteorological parameters (pressure, temperature, relative humidity, wind speed and direction) were attached to a helium-filled tethered balloon, with a volume of 30 m^3 and a payload weight of 10 kg. The fish-shaped balloon was well balanced during launches, thus the disturbance imposed on instruments by ascents and descents of the balloon could be largely minimized. Launches were scheduled every 3 hours between 06:00 and 21:00 (Local Time, LT) from the ground to 1 km height. However, feasible launches actually depended upon wind speed and the precipitation, as well as air traffic control. In total, 48 successful launches were conducted on 15 days, of which 40 reached above 0.5 km. Through the entire field campaign, 89 vertical profiles of BC were reliably obtained. Lack of data for several ascending or descending processes was primarily caused by discarding invalid data under wind gusts, which led to the violent swing of the tethered balloon and poor data quality. The balloon ascended at a rate of 1 m s^{-1} and descended at a rate of 0.5 m s^{-1} under the control of an electric winch. With a sampling interval of 1 s for all instruments, the observational vertical resolution was ~1 m. For analysis in this study, 20-m averaged data were used.

AE-51 operated with a similar principle of the aethalometer as described in Hansen et al. (1984). The intensity of transmitted light through a 3-mm diameter sample spot (I) and an aerosol-free reference spot (I_0) on a T60 Teflon-coated borosilicate glass fiber filter were simultaneously detected to obtain attenuation coefficients at the wavelength of 880 nm ($\sigma_{\text{AE-51,880nm}}$) following:

$$\sigma_{\text{AE-51,880nm}} = \frac{A \times \Delta\text{ATN}}{100 \times F \times \Delta t}, \quad (1)$$

where A is the area of the aerosol collecting spot (0.071 cm^2), F is the flow rate (150 ml min^{-1}), ATN denotes light attenuation and calculated from $100 \times \ln(I_0/I)$, ΔATN is the change of ATN during the sampling interval Δt (1 s). A homemade silica gel dryer was placed in front of the inlet to efficiently dry ambient aerosols. A test on the dryer was performed before the campaign to ensure the duration and efficiency of its usage.

2.3 Data processing

2.3.1 The smoothing algorithm

At a high temporal resolution of 1 s, steady increase of ATN with sampling time was not as usually found due to instrumental noises. Acquired data was consisted of many large values with positive or negative signs. A post-processing method, Optimized Noise-reduction Averaging (ONA) algorithm, has been developed by Hagler et al. (2011), where adaptive time-averaging of the BC data was conducted with the time window of averaging optimally chosen by ΔATN. In

删除的内容: 1
删除的内容: s
删除的内容: destabilization
删除的内容: m/s
删除的内容: m/s
删除的内容: estimate aerosol absorption
删除的内容: 2
删除的内容: 2
删除的内容: S

this study, data dispersion due to high temporal resolution was treated by a new smoothing algorithm. Fluctuation Minimizing Smoothing (FMS). Similar to the ONA method, the FMS approach is also principally based upon the physical behavior of measured ATN. Despite that BC values determined from fluctuated ATN might drastically vary, large positive/negative pairs of BC values would always be found and counterbalance each other within a few seconds. Therefore, the FMS approach was devised to find pairs of BC values that differ largely with each other within a few seconds and make a compromise. The procedure was performed as following:

(1) For each data point x_i of a continuously measured time series with N records, calculate the difference between x_i and all other data points within n seconds to generate a matrix of $D_{i,j}=|x_i-x_{i+j}|$, where $i=1,2,\ldots,N-1,N$ and $j=1,2,\ldots,n-1,n$;

(2) Find the largest value of the matrix $D_{k,l}$, which is the difference between point x_k and x_{k+l};

(3) Replace x_k and x_{k+l} with $(x_k+x_{k+l})/2$ and set $D_{k,l}$ to a minus number;

(4) Replace any $D_{i,j}$ that has been calculated using x_k or x_{k+l}, except for $D_{i,j}$ with a minus number. This step is optional, since it largely raises the computational cost;

(5) Repeat step (2)-(4) until no positive numbers in the matrix;

(6) Repeat step (1)-(5) for m times to obtain acceptable smoothed data.

The smoothing window n and the smoothing count m were empirically chosen during the calculation. It should be kept in mind that using improper large n or m might wipe off some natural variations, although it will always give a smoother result. n should be set to no more than 5, given that data fluctuation is normally already compensated within 5 s. With n to be 5 and m to be 1, the average of the target point was mostly contributed from neighboring data points within about 11 seconds, according to a weight of 80%. This consequently led to a vertical resolution of about 22 m for the ascent and 11 m for the descent after smoothing. Similarly, the vertical resolution was about 50~60 m for the ascent and 25~30 m for the descent when m was set to be 5. Different choices of m gave a similar pattern of vertical profiles, but with some differences in details. In this study, m was set to be 5 to achieve a better smoothing for further calculations, though this caused a loss of the vertical resolution more than twice as large as that when just smoothing once. A comparison was made between unsmoothed data, smoothed data using the FMS approach in this study and the ONA method in Hagler et al. (2011), as well as 20-m averaged data using those two algorithms. It was found that both algorithms could properly deal with data fluctuation caused by instrumental noises without introducing artificial features (e.g., Fig. 3a-3c). However, the FMS method seemed to be more capable of reliably removing outliers in some cases (e.g., Fig. 3d-3f). The comparison indicated that the FMS procedure could effectively reduce data fluctuation while still preserve reasonable variability of the profile.

2.3.2 The correction method

Measured $\sigma_{AE\text{-}51,880nm}$ suffered from systematic biases introduced by the filter-based technique. In order to determine BC absorption coefficients (σ_{BC}) from $\sigma_{AE\text{-}51,880nm}$, corrections were required to tackle with three types of artifacts. The shadowing effect, an artifact that results in gradual artificial reduction in $\sigma_{AE\text{-}51,880nm}$ due to the saturation of the filter with increasing aerosol loading, leads to an underestimation of σ_{BC} and a discontinuity after changing to a new sample spot

删除的内容: .

删除的内容: -n

删除的内容: -n+1

删除的内容: smoothing window

删除的内容: smoothing count

删除的内容: s are

删除的内容: The smoothing count m is set to be 5 in this study. A comparison made between smoothed data using our algorithm and the method in Hagler et al. (2011) indicated that our procedure reduced more fluctuations and kept reasonable variations of the data.

删除的内容: 2

删除的内容: C

删除的内容: of absorption coefficients

删除的内容: inherent in

删除的内容: , including an underestimation due to loading effect and an overestimation due to aerosol scattering and multiple scattering of filter fibers

(Weingartner et al., 2003). Various methods have been developed to address the shadowing effect (Weingartner et al., 2003; Virkkula et al., 2007; Ran et al., 2016). However, this artifact could be neglected in this study, since no ATN exceeded 20 with a new filter for each launch. The other two artifacts cause an overestimation of σ_{BC} by enhancing light attenuation, either due to aerosol scattering or the multiple scattering of filter fibers (Weingartner et al., 2003; Arnott et al., 2005; Schmid et al., 2006; Collaud Coen et al., 2010). A correction factor (C) was needed to correct these two artifacts.

The C factor was derived from a surface comparative test for about 1 week in Beijing among AE-51, a 7-wavelength aethalometer (Model AE-31, Magee Scientific, USA) and a multi-angle absorption photometer (MAAP, Model 5012, Thermo, USA). Continuous operation of AE-51 was carried out in order to obtain a proper size of the dataset in limited time period, despite that AE-51 is in principle not designed to be operated around the clock. A daily check of the flow rate was performed using a Gilibrator-2 Diagnostic Kit (Sensidyne, USA) to ensure the stability of the flow and thus data quality.

AE-31 suffered instrumental artifacts in the same way as AE-51. Details of the correction scheme developed for tackling with AE-31 artifacts were described in Ran et al. (2016). Briefly, the correction scheme combined the modified Virkkula method (Virkkula et al., 2007) to treat the shadowing effect and the Schmid method (Schmid et al., 2006) to treat filter multiple scattering and aerosol scattering effects. The modified Virkkula method assumed a linear relationship of BC mass concentrations and time across the filter change, particularly, a quadratic relationship for special cases where ambient BC experienced a peak-shaped variation, instead of constant BC mass concentrations as in Virkkula et al. (2007). The wavelength-dependent correction factor (C_λ) could be obtained following procedures in Schmid et al. (2006). The temporal resolution of AE-31 during the comparative test was 2 min.

MAAP continuously measured aerosol absorption coefficients at the actual wavelength of 637 nm ($\sigma_{MAAP,637nm}$) instead of the nominal wavelength of 670 nm (Müller et al., 2011), with a temporal resolution of 1 min. Multi-angle detections of the transmittance and reflectance, as well as a two-stream approximation in the radiative transfer scheme adopted by MAAP have significantly improved measurements of ambient aerosol absorption coefficients (Petzold and Schönlinner, 2004; Petzold et al., 2005). Hyvärinen et al. (2013) reported an artifact of underestimated BC mass concentrations after a spot change and attributed it to yet unconfirmed causes as erroneous dark counts in the transmitted light photodetector and an instrument internal averaging procedure of the photodetector raw signals. It was stated that this artifact could be observed with a BC mass accumulation rate, as the product of BC mass concentrations and the flow rate of MAAP, larger than 0.04 μg min^{-1}, which corresponds to 3 μg m^{-3} at the flow rate of 1 m^3 h^{-1}. However, no apparent underestimation of BC mass concentrations was found in this study, even for cases where BC mass concentrations exceeded 8 ug m^{-3} (Fig. S2). Consequently, measured $\sigma_{MAAP,637nm}$ without any corrections were used for subsequent calculations and taken as real values.

Three steps were taken to obtain the C factor. Firstly, aerosol absorption Angström exponent (α) over the spectrum span of 660 and 880 nm was derived from absorption coefficients $\sigma_{AE\text{-}31,660nm}$ and $\sigma_{AE\text{-}31,880nm}$, which were corrected from attenuation coefficients at 660 and 880 nm measured by AE-31. Hence, α was calculated from:

$$\alpha = \frac{\ln(\sigma_{AE\text{-}31,660nm}) - \ln(\sigma_{AE\text{-}31,880nm})}{\ln(880) - \ln(660)}. \quad (2)$$

已下移 [1]: (Weingartner et al., 2003; Arnott et al., 2005; Schmid et al., 2006; Collaud Coen et al., 2010).

删除的内容:

删除的内容:

删除的内容: With a new filter for each launch, loading effect, a saturation-induced reduction in the optical path along with increasing aerosol loading,

带格式的: 英语(美国)

已移动(插入) [1]

已下移 [2]: Hence, mass concentrations of BC (m_{BC}) could be directly converted from $\sigma_{AE\text{-}51,880nm}$ using the documented 'specific attenuation' of 12.5 (m^2 g^{-1}), considering that BC is the major contributor to aerosol absorption at 880 nm (Ramachandran and Rajesh, 2007).

删除的内容: .

删除的内容: The determination of BC absorption coefficients (σ_{BC}) from $\sigma_{AE\text{-}51,880nm}$ required a correction for aerosol scattering and multiple scattering of filter fibers. The correction factor (C) used to correct these artifacts

删除的内容: on basis of

删除的内容: 1-week

删除的内容: Aerosol absorption coefficients at 670 nm ($\sigma_{MAAP,670nm}$) were measured by MAAP.

删除的内容: Thereby, $\sigma_{MAAP,670nm}$ were taken as real values for subsequent corrections.

删除的内容: A

删除的内容: needed for estimating $\sigma_{MAAP,880nm}$ was calculated from absorption coefficients at 660 nm ($\sigma_{AE\text{-}31,660}$) and 880 nm ($\sigma_{AE\text{-}31,880}$),

删除的内容: measurements of AE-31:

Secondly, α for the spectrum of 660 and 880 nm was used to represent α over the span of 637 and 880 nm. Therefore, $\sigma_{MAAP,880nm}$ was quantified from measured $\sigma_{MAAP,637nm}$ following the spectral dependence of aerosol absorption coefficients in the form of $\lambda^{-\alpha}$:

$$\sigma_{MAAP,880nm} = \sigma_{MAAP,637nm} \times (\frac{880}{637})^{-\alpha}, \quad (3)$$

Finally, reduced major axis regression of attenuation coefficients $\sigma_{AE-51,880nm}$ (ATN<10) measured by AE-51 and absorption coefficients $\sigma_{MAAP,880nm}$ calculated from MAAP and AE-31 yielded the *C* factor of 2.98±0.05 with 95% confidence (Fig. 2). It was noted that the *C* factor for AE-51 was reported as 2.05±0.03 with 95% confidence in Ferrero et al. (2011a). Possible explanations on such a difference in the *C* factor might be found in aerosol chemical compositions in the NCP region and the Po Valley basin. Besides, the *C* factor in Ferrero et al. (2011a) was obtained from Mie calculations, and thus was subject to uncertainties resulting from assumptions such as BC size distributions, BC mixing state and particle morphology. In addition, the choice of the correction scheme for AE-31 measurements in this study might introduce uncertainties to α and thereby $\sigma_{MAAP,880nm}$. Using a constant *C* factor for AE-31 as also often used in some studies (e.g., Weingartner et al., 2003; Sandradewi et al., 2008) instead of the wavelength-dependent C_λ results in an underestimation of α over the 660-880 nm spectrum by about 19.5%. This consequently leads to an overestimation of $\sigma_{MAAP,880nm}$ and the *C* factor for AE-51 by about 9.6% and 8.4%, respectively. By dividing *C* into $\sigma_{AE-51,880nm}$, absorption coefficients σ_{BC} could be estimated. As for the mass concentration of BC (m_{BC}), it could be directly converted from $\sigma_{AE-51,880nm}$ using the documented 'specific attenuation' of 12.5 m^2 g^{-1} considering that BC is the major contributor to aerosol absorption at 880 nm (Ramachandran and Rajesh, 2007).

2.3.3 The calculation of meteorological parameters

Instead of measured temperature (*T*) and relative humidity (RH), two conservative quantities, potential temperature (θ) and specific humidity (*q*) were used to provide information on the evolution of PBL. The calculation of θ (K) followed:

$$\theta = T \times (p_0 / p)^{R_d / C_{pd}}, \quad (4)$$

where p and p_0 are respectively measured pressure and the standard pressure at the sea level (hPa), T is measured temperature (K), R_d is the individual gas constant for dry air (287 J kg^{-1} K^{-1}), C_{pd} is the specific heat at constant pressure for dry air at the standard temperature (1005 J kg^{-1} K^{-1}). Calculated θ was then expressed in degree Celsius (^oC) in order to be straightforward. Specific humidity (q, g kg^{-1}) was calculated from:

$$q = \varepsilon \times \frac{e}{p - (1-\varepsilon) \times e} \times 1000, \quad (5)$$

where ε is the ratio of the molecular weight of water vapour to that of dry air (0.622), e is the vapour pressure of water (hPa), which is the product of measured RH (%) and calculated water saturation pressure (e_s) at each measured temperature T.

删除的内容: Details of the correction scheme developed for tackling with artifacts of AE-31 were described in Ran et al. (2016).

删除的内容: F

删除的内容: , $\sigma_{MAAP,880nm}$ could be quantified from $\sigma_{MAAP,670nm}$ by

删除的内容: $\sigma_{MAAP,880nm} = \sigma_{MAAP,670nm}$

域代码已更改

删除的内容: Measured

删除的内容: and calculated

删除的内容: were linearly fitted with a correlation coefficient of 0.96 in a significant level (P<0.001), yielding a *C* value of 2.52.

已移动(插入) [2]

删除的内容: Hence, mass concentrations of BC (m_{BC})

删除的内容: (

删除的内容:)

删除的内容: 2

删除的内容: C

3 Results and Discussion

3.1 Vertical distributions of BC and meteorological parameters

A set of 67 vertical profiles of BC and meteorological parameters were selected. The mixing layer (ML) could be clearly discerned for profiles measured in the daytime. Exceptions were those measured around noon, when the top of the ML, often higher than 1 km in summer, was beyond reach of the tethered balloon. In addition, several launches took place in the evening to observe BC vertical distributions shaped by the nocturnal boundary layer (NBL). A statistical summary of the field campaign and the meteorology is given in Table 1. Most profiles were sampled under mild winds in the morning and evening, when relatively stable conditions suitable for launches of the tethered balloon were more easily encountered. Air masses were mainly carried, either by southeasterly or southwesterly winds, from areas densely populated and heavily industrialized, also ramified with railways and highroads.

Figure 4 illustrates an example of vertical distributions of BC, θ, q, and winds during one launch on July 8, 2014 (10:41-11:27 LT). 20-m averaged data are denoted by dots in dark color for the ascent and light color for the descent. Arrows depict vector mean horizontal winds, with the length to represent wind speed and the arrowhead to give wind direction following meteorological definitions. The height of a clearly defined ML was marked by a solid line for each BC vertical profile. A nearly uniform distribution of BC, as well as θ and q, was observed within the strongly convective ML. Large vertical gradient of m_{BC} across entrainment layer (EL) led to approximately 50% reduction from the level in the ML to that in free troposphere (FT). Concomitantly, a substantial reduction in q, whereas an increase in θ, was also immediately found above the ML. The difference in profiles between the ascent and the descent evidently indicated a rapid evolution of the ML near noon and its impact on vertical distributions of BC and meteorology. More discussions regarding diurnal variations of BC vertical profiles will be found in next section.

The mixing height could be determined by applying the gradient method to the entire dataset (Seibert et al., 2000; Kim, et al., 2007). Generally, the mixing height determined from profiles of m_{BC} ($H_{m,BC,gradient}$) agreed well with that from profiles of θ ($H_{m,\theta}$) and q ($H_{m,q}$) as shown in Fig. S3. The reliability of estimating the mixing height from vertical measurements of BC had also been demonstrated in previous studies (Ferrero et al., 2010; Ferrero et al., 2011b). On the other hand, typical daytime profiles of m_{BC} could be well characterized by the sigmoid function:

$$m_{BC} = C_{ms} - \frac{C_{ms} - C_{fs}}{e^{-(h-H_{m,BC,sigmoid})/H_e} + 1}, \quad (6)$$

where C_{ms} and C_{fs} are respectively characteristic m_{BC} within the ML and in FT, $H_{m,BC,sigmoid}$ is the mixing height derived from BC vertical profiles using the sigmoid function, H_e represents the thickness of the EL, h is the height at which each 20-m averaged m_{BC} is obtained. The parameters C_{ms}, C_{fs}, $H_{m,BC,sigmoid}$ and H_e could be directly determined by fitting measured m_{BC} at each height h using Eq. (6) as shown by the example (Fig. S4). A comparison was made between $H_{m,BC,gradient}$ and $H_{m,BC,sigmoid}$ for typical daytime BC vertical profiles. Results from the two methods agreed quite well with each other, with a difference of less than 2 % (Fig. S5). In addition to reliably estimating the mixing height as the gradient method, the sigmoid

删除的内容: 1

删除的内容: (H_m)

已移动(插入) [3]

已移动(插入) [4]

删除的内容: H_m

删除的内容: H_m was calculated from a sigmoid function that could well characterize typical daytime profile of m_{BC}: . $m_{BC} = C_{ms} - \frac{C_{ms} - C_{fs}}{e^{-(h-H_m)/H_e} + 1}$

域代码已更改

删除的内容: the free troposphere (

删除的内容:)

删除的内容: entrainment layer (

删除的内容:)

删除的内容: H_m determined from profiles of θ and q generally agreed well with that from profiles of m_{BC}.

function could also directly determine parameters including C_{ms}, C_{fs}, and H_s. Therefore, the sigmoid function was chosen to obtain all parameters for typical daytime BC profiles. As for non-typical daytime BC profiles, either as a result of a polluted layer in FT or barely sufficient height into FT reached by the tethered balloon, a sigmoid function was not applicable and the gradient method was used to estimate the mixing height. Near sunset, the NBL forms along with the collapse of the ML (Kaimal and Finnigan, 1994; Lazaridis, 2011). The structure of the NBL is more complicated and the determination of the NBL height bears more uncertainty (Yu, 1978; Poulos, et al., 2002). A subjective procedure based on the gradient method was utilized to estimate the NBL height. In summary, the mixing height determined from vertical profiles of BC, either by the gradient method or the sigmoid function, as well as the estimated NBL height, were denoted as H_m in this study for convenience.

Table 2 summaries calculated parameters for BC vertical profiles during different periods. Average m_{BC} within the ML and in FT were denoted as C_m and C_f, which were C_{ms} and C_{fs} for typical daytime BC profiles. As for non-typical daytime BC profiles, C_m was the average of m_{BC} below H_m. When H_m exceeded 1 km, m_{BC} measured along the ascending/descending path from the ground to the maximum height reached by the tethered balloon were averaged to obtain C_m. For NBL cases, only C_f was obtained by averaging m_{BC} above H_m. A large variability was found in C_m, with a range of 1.12 to 14.49 μg m^{-3}. On average, C_f stayed relatively steadily, though it ranged from 0.36 μg m^{-3} in clean cases to 3.14 μg m^{-3} under polluted conditions.

Statistically, vertical profiles of BC were categorized into two types, according to their shapes along the normalized height (H_{Nor}), which was calculated from h/H_m-1 (Ferrero et al., 2014). H_{Nor} shows the surface with a value of -1 and the top of the ML with a value of 0. One type of BC vertical profiles, exclusively measured in the daytime, displayed a vertical distribution typically shaped by a well-mixed mixing layer (Fig. 5a). BC almost uniformly distributed within the ML, in a similar way as the example (Fig. 4), with an average m_{BC} level of about 5.16±2.49 μg m^{-3}, or σ_{BC} of about 21.64±10.45 Mm^{-1}. This is comparable with what has been observed within the PBL in many polluted urban areas (Table 3). A couple of highly polluted cases, where C_m exceeded 10 μg m^{-3}, were observed in the early morning. The formation of the convective ML just started at that time and vertical turbulence was yet not strong enough to dilute the high level of BC, which was primarily emitted near the ground and accumulated within the stable NBL over night. Due to a sharp reduction in m_{BC} from the ML to FT, average C_f was about 1.61±0.94 μg m^{-3}. The second type of BC vertical profiles revealed the feature of trapped air pollutants in the shallow stable NBL. For each BC profile (grey lines in Fig. 5b), m_{BC} nearly exponentially declined with H_{Nor}, as a result of weakened turbulence and vertical dispersion. Under polluted conditions, C_f could reach as high as 2.83 μg m^{-3}, otherwise usually well below 1 μg m^{-3}.

3.2 Diurnal variations of BC vertical profiles

An investigation on diurnal variations of BC vertical profiles was able to be undertaken on July 1, 8, and 13, when measurements generally covered the period from early morning to afternoon or evening. On other observational days, the dataset was incomplete due to aborted launches under strong winds or precipitation. For clarity, only the vertical profile

已移动(插入) [5]

删除的内容: vertical

已移动(插入) [6]

删除的内容: H_m (Seibert et al., 2000; Kim, et al., 2007)

删除的内容: r

删除的内容: , which was also denoted as H_m in this study for convenience

已上移 [4]: The reliability of estimating H_m from vertical measurements of BC had also been demonstrated in previous studies (Ferrero et al., 2010; Ferrero et al., 2011b).

已上移 [3]: A nearly uniform distribution of BC, as well as θ and q, was observed within the strongly convective ML. Large vertical gradient of m_{BC} across EL led to approximately 50% reduction from the level in the ML to that in FT. Concomitantly, a substantial reduction in q, whereas an increase in θ, was also immediately found above the ML. The difference in profiles between the ascent and the descent evidently indicated a rapid evolution of the ML near noon and its impact on vertical distributions of BC and meteorology. More discussions regarding diurnal variations of BC vertical profiles will be found in next section.

删除的内容: the

删除的内容: vertical

已上移 [5]: As for non-typical BC vertical profiles, either as a result of a polluted layer in FT or barely sufficient height into FT reached by the tethered balloon, a sigmoid function was not applicable and the gradient method was used to estimate H_m (Seibert et al., 2000; Kim, et al., 2007).

删除的内容: value

已上移 [6]: Near sunset, the NBL forms along with the collapse of the ML (Kaimal and Finnigan, 1994; Larzridis, 2011). Th...

删除的内容: O

删除的内容: from

删除的内容: for such cases

删除的内容: H_m could not be determined when exceeding 1 km as above stated. ...

删除的内容: 2a

删除的内容: 1

删除的内容: 25.60

删除的内容: 12.35

during the descent of each launch is plotted in Fig. 6. Additionally, profiles not included into the selected dataset are also shown.

A distinct diurnal variation was found both in the shape of BC vertical profiles and the level of m_{BC} along the profile. To a great extent, the diurnal cycle of BC vertical profiles followed the evolution of the ML. In the early morning, BC was largely restricted within a thin ML less than 0.2 km above the ground when vertical turbulence was still weak. m_{BC} dropped dramatically from a high level within the ML to a significantly low level above the ML, even less than 10% as could be found on July 13. In polluted cases, however, m_{BC} in FT could exceed 2 μg m^{-3} and sometimes reach nearly 50% of that at the surface (e.g., profiles on July 1 and 8). This might imply the existence of a polluted residual layer above the stable surface layer formed after the sunset in previous evening, yet unable to be further discussed without continuous measurements from the day before. Also the characteristics of m_{BC} in FT should be affected by the advection. After sunrise, vertical turbulence in the ML gradually strengthened as the earth was continuously heated by solar radiation. The convective ML developed quickly in the forenoon, with elevated H_m and decreased C_m. Marked changes in BC vertical profiles could be observed even during one launch when the mixing height rose so rapidly, as shown in the example (Fig. 4). The maximum height of the ML commonly exceeded 1 km in the afternoon during the field campaign (e.g., profiles on July 8), except on cloudy days when the ML did not fully develop. As the evening approached, convection abruptly decayed and a stable NBL began to form. m_{BC} in FT promptly declined to its typical level, often leaving no trail to indicate the daytime mixing with polluted air masses beneath. In contrast, air pollutants including BC quickly built up in the shallow NBL. Sometimes, a residual layer with a relatively high level of m_{BC} (>2 μg m^{-3}) could be formed above the NBL where the remnant of the daytime mixing layer might be traced after its collapse (e.g., profiles on July 8). This would undoubtedly have an impact on measured m_{BC} above the mixing layer on the next day, leading to a polluted background in FT (e.g., in the morning of July 1 and 8). The role of the residual layer in affecting the evolution of the PBL still stays controversial, though it has been consented that BC could heat the PBL and intensify atmospheric stability. Ding et al. (2016) demonstrated the importance of the "dome effect" of BC in the PBL especially the upper PBL, suppressing the PBL height and enhancing haze pollution within a lower PBL. Whereas in Zhang et al. (2012), a limited warming effect of BC in an elevated aerosol layer and limited induced increase in the strength of atmospheric inversion were indicated.

It was interestingly noticed that a polluted layer with a thickness of about 0.3 km, extending from the height of 0.2 km to 0.5 km, lay right above the ML in the early morning on July 1. The polluted layer could also be accordingly recognized from meteorological features of more moisture and wind shear across its boundaries. Wind direction was southeast in the ML and FT, while southwest in the polluted layer. Average m_{BC} within the polluted layer was about 4 μg m^{-3}, half of that near the surface and double of that in FT. Actually, the vertical profile within the morning ML quite resembled characteristics of a nocturnal profile even though the sun had risen, suggesting that strong inversion of the NBL still overrode weak vertical turbulence at that time. As surface emissions from human activities kept increasing, m_{BC} within the ML elevated. Further development of vertical convection broke the layered structure, leading to the merge of the polluted layer and the ML.

删除的内容: 3

删除的内容: 00

删除的内容:

删除的内容: Gradually

删除的内容: after sunrise

删除的内容: 1

Slowly, the polluted layer vanished into the convective ML, though remained until 9:00 LT in the morning. An elevated aerosol layer (0.7~1 km), in which BC was well aged, has previously been observed in the afternoon over Beijing by Zhang et al. (2012), and was attributed to the residual nocturnal stable layer. Possible origin of the polluted layer present here and the status of BC in the layer were unable to be decided on basis of limited observations. Nonetheless, a higher q in the polluted layer than at the surface and different wind direction might imply an elevated residual layer formed after sunset on the day before and transported from somewhere else. It was quite cloudy and sultry during the daytime, and a heavy rainfall occurred near the evening. Thus, the top of the ML was still below 0.5 km when the launch was carried out around noon. Despite that the tethered balloon failed to reach 1 km due to strong winds aloft, a part of a relatively polluted layer with apparent increase in moisture and potential temperature could be roughly distinguished. Wind direction in the polluted layer was southwest, whereas predominant wind direction beneath had changed to southeast. The polluted layer, extending from about 0.7 km to the top of the reachable height, disappeared during the last launch around 14:00 LT on that day and was probably a transported plume.

Figure 7 displays H_m and m_{BC} from the entire selected dataset on a diurnal scale. Observations on each day are shown in one color. Variations in H_m through the field campaign generally resembled the diurnal cycle observed on an individual day (Fig. 7a). The ML, though still shallow, developed slowly after sunrise. In addition to a high level of BC trapped near the ground by the stable NBL, fresh emissions from daytime human activities further aggravated surface pollution. Observed m_{BC} was usually quite high in the early morning, sometimes even experienced an increase with time, depending upon how fast the ML developed and emissions increased. The thickening of the mixing depth accelerated in late morning on sunny days, whereas impeded on cloudy days only to form a thin mixing layer. Accordingly, C_m (solid dots in Fig. 7b) largely reduced from morning to noon in strongly convective ML on sunny days, however, stayed relatively stable through morning on cloudy days. Comparative cases could be found on July 1 and 14. Based on current knowledge of the boundary layer, the maximum height of the ML on sunny days would be reached in late afternoon, but could not be observed in this study since it was well above the flight limit of the tethered balloon. The collapse of the ML was not directly captured. However, intensive measurements favored by the meteorology on July 8 revealed that the convective ML quickly faded away on a time scale of 1 hour near sunset. Instead, a stable and shallow NBL confined nighttime emissions near the ground, giving rise to enhanced surface pollution (open dots in Fig. 7b).

删除的内容: 4

删除的内容: 4a

删除的内容: 4b

删除的内容: 4b

4 Conclusions

In-situ measurements of black carbon (BC) vertical profiles were carried out at a semirural site during the VOGA 2014 summer field campaign, using a micro-aethalometer attached to a tethered balloon system. A set of 67 BC vertical profiles was reliably collected and diurnal variations of BC vertical profiles were examined.

Vertical distributions of BC and meteorological parameters, as well as the mixing height (H_m) identified from BC profiles, experienced a distinct diurnal cycle guided by the development of the mixing layer (ML). In the morning, weak turbulence

within the shallow ML (thinner than 0.2 km) favored the accumulation of enhanced surface emissions, sometimes leading to a severe pollution with BC mass concentrations (m_{BC}) exceeding 10 μg m^{-3}. The high level of BC within the ML was diluted with the fast development of a strongly convective ML. H_m reached its maximum in late afternoon and exceeded 1 km on sunny days, whereas stayed much lower on cloudy days. Typically in the daytime, BC uniformly distributed within the ML and sharply decreased above the ML to a level even less than 10% of that near the surface. Average m_{BC} within the ML (C_m) was about 5.16±2.49 μg m^{-3} over the entire field campaign, with a range of 1.12 to 14.49 μg m^{-3}, comparable with what has been observed in many polluted urban areas. C_f, average m_{BC} in free troposphere (FT), was below 1 μg m^{-3} under clean conditions and amounted to half of the ground level under pollution conditions. In the evening, BC quickly built up near the surface and exponentially declined with height, following the collapse of the ML and the formation of a stable nocturnal boundary layer (NBL). Particularly, two polluted layers were observed at different time and heights on July 1. Origins of the polluted layers were not able to be evidently decided. However, the presence of BC polluted layers in FT, either as an elevated residual layer in the morning or a transported plume in the afternoon as suggested by the history of the layer and the meteorology, might considerably influence direct radiative forcing by BC and atmospheric stability.

Acknowledgements

This research was funded by the National Natural Science Foundation of China (NSFC) under Grant No. 41305114, 41205098, 41330442 and 41127901. This work was also supported by China Special Fund for Meteorological Research in the Public Interest (No. GYHY201206015). We are grateful to Yong Wang, Chuncheng Ji, Qihua Du, Hanze Yu and Xinpan Li for their cooperation in launching the tethered balloon. We also thank Raoyang Meteorological Bureau for providing the location for our measurements. The Terra and Aqua/MODIS Aerosol Level 2 Products were acquired from the Level-1 & Atmosphere Archive and Distribution System (LAADS) Distributed Active Archive Center (DAAC), located in the Goddard Space Flight Center in Greenbelt, Maryland (https://ladsweb.nascom.nasa.gov/). The 2012 multi-resolution emission inventory for China (MEIC, http://www.meicmodel.org) was obtained from the MEIC team.

Appendix A Nomenclature Table

Symbol	Definition
α	Aerosol absorption Angström exponent, here calculated from $\sigma_{\text{AE-31,660nm}}$ and $\sigma_{\text{AE-31,880nm}}$
$\sigma_{\text{AE-31,660nm}}$	Aerosol absorption coefficient measured by AE-31 at the wavelength of 660 nm
$\sigma_{\text{AE-31,880nm}}$	Aerosol absorption coefficient measured by AE-31 at the wavelength of 880 nm
$\sigma_{\text{MAAP,670nm}}$	Aerosol absorption coefficient measured by MAAP at the wavelength of 670 nm
$\sigma_{\text{MAAP,880nm}}$	Aerosol absorption coefficient at the wavelength of 880 nm, calculated from α and $\sigma_{\text{MAAP,670nm}}$
$\sigma_{\text{AE-51,880nm}}$	Aerosol absorption coefficient measured by AE-51 at the wavelength of 880 nm
σ_{BC}	Absorption coefficient of black carbon at the wavelength of 880 nm
λ	Wavelength
θ	Potential temperature
ATN	Light attenuation
C	Correction factor for filter multiple scattering and aerosol scattering
C_{f}	Average m_{BC} in the free troposphere
C_{m}	Average m_{BC} within the mixing layer
C_{fs}	Characteristic m_{BC} in the free troposphere, derived from sigmoid fitting
C_{ms}	Characteristic m_{BC} within the mixing layer, derived from sigmoid fitting
H_{e}	The thickness of the entrainment layer, derived from sigmoid fitting
H_{m}	The height of the mixing layer, also used to denote the height of the NBL layer in this study
$H_{\text{m,BC,gradient}}$	The height of the mixing layer estimated from the vertical profile of BC using the gradient method
$H_{\text{m,BC,sigmoid}}$	The height of the mixing layer estimated from the vertical profile of BC using the sigmoid function
$H_{\text{m},\theta}$	The height of the mixing layer estimated from the vertical profile of θ using the gradient method
$H_{\text{m,q}}$	The height of the mixing layer estimated from the vertical profile of q using the gradient method
H_{Nor}	The normalized height, defined as h/H_{m}-1
m_{BC}	Mass concentration of black carbon, converted from $\sigma_{\text{AE-51,880nm}}$
q	Specific humidity
RH	Relative humidity
T	Temperature

References

Andreae, M. O.: The dark side of aerosols, Nature, 409, 671-672, 2001.

Arnott, W. P., Hamasha, K., Moosmuller, H., Sheridan P. J., and Ogren J. A.: Towards aerosol light-absorption measurements with a 7-wavelength aethalometer: evaluation with a photoacoustic instrument and 3-wavelength nephelometer, Aerosol Sci. Tech., 39, 17-29, doi:10.1080/027868290901972, 2005.

Babu, S. S., Sreekanth, V., Moorthy, K. K., Mohan, M., Kirankumar, N. V. P., Subrahamanyam, D. B., Gogoi, M. M., Kompalli, S. K., Beegum, N., Chaubey, J. P., Kumar, V. H. A., and Manchanda, R. K.: Vertical profiles of aerosol black carbon in the atmospheric boundary layer over a tropical coastal station: Perturbations during an annular solar eclipse, Atmos. Res., 99. 471-478, doi:10.1016/j.atmosres.2010.11.019, 2011a.

Babu, S. S., Moorthy, K. K., Manchanda, R. K., Sinha, P. R., Satheesh, S. K., Vajja, D. P., Srinivasan, S., and Kumar, V. H. A.: Free tropospheric black carbon aerosol measurements using high altitude balloon: Do BC layers build "their own homes" up in the atmosphere?, Geophys. Res. Lett., 38, L08803, doi:10.1029/2011GL046654, 2011b.

Ban-Weiss, G. A., Cao, L., Bala, G., and Caldeira, K.: Dependence of climate forcing and response on the altitude of black carbon aerosols, Clim. Dyn., 38, 897-911, doi:10.1007/s00382-011-1052-y, 2012.

Bond, T. C., Habib, G., Bergstrom, R. W.: Limitations in the enhancement of visible light absorption due to mixing state, J. Geophys. Res., 111, D20211, doi:10.1029/2006JD007315, 2006.

Bond, T. C., Doherty, S. J., Fahey, D. W., Forster, P. M., Berntsen, T., DeAngelo, B. J., Flanner, M. G., Ghan, S., Kärcher, B., Koch, D., Kinne, S., Kondo, Y., Quinn, P. K., Sarofim, M. C., Schultz, M. G., Schulz, M., Venkataraman, C., Zhang, H., Zhang, S., Bellouin, N., Guttikunda, S. K., Hopke, P. K., Jacobson, M. Z., Kaiser, J. W., Klimont, Z., Lohmann, U., Schwarz, J. P., Shindell, D., Storelvmo, T., Warren, S. G., and Zender, C. S.: Bounding the role of black carbon in the climate system: a scientific assessment, J. Geophys. Res., 118, 5380-5552, doi:10.1002/jgrd.50171, 2013.

Chen, J., Zhao, C. S., Ma, N., Liu, P. F., Göbel, T., Hallbauer, E., Deng, Z. Z., Ran, L., Xu, W. Y., Liang, Z., Liu, H. J., Yan, P., Zhou, X. J., and Wiedensohler, A.: A parameterization of low visibilities for hazy days in the North China Plain, Atmos. Chem. Phys., 12, 4935-4950, doi:10.5194/acp-12-4935-2012, 2012.

Collaud Coen, M., Weingartner, E., Apituley, A., Ceburnis, D., Fierz-Schmidhauser, R., Flentje, H., Henzing, J. S., Jennings, S. G., Moerman, M., Petzold, A., Schmid, O., and Baltensperger, U.: Minimizing light absorption measurement artifacts of the aethalometer: evaluation of five correction algorithms, Atmos. Meas. Tech., 3, 457-474, doi:10.5194/amt-3-457-2010, 2010.

Corrigan, C. E., Roberts, G. C., Ramana, M. V., Kim, D., and Ramanathan, V.: Capturing vertical profiles of aerosols and black carbon over the Indian Ocean using autonomous unmanned aerial vehicles, Atmos. Chem. Phys., 8, 737-747,

删除的内容:

删除的内容:

doi:10.5194/acp-8-737-2008, 2008.

Ding, A. J., Huang, X., Nie, W., Sun, N. J., Kerminen, V. M., Petäjä, T., Su, H., Cheng, Y. F., Yang, X. Q., Wang, M. H., Chi, X. G., Wang, J. P., Virkkula, A., Guo, W. D., Yuan, J., Wang, S. Y., Zhang, R. J. Zhang, Wu, Y. F., Song, Y. Song, Zhu, T., Zilitinkevich, S., Kulmala, M., and Fu, C. B.: Enhanced haze pollution by black carbon in megacities in China, Geophys. Res. Lett., 43, 2873-2879, doi:10.1002/2016GL067745, 2016.

Ferrero, L., Perrone, M. G., Petraccone, S., Sangiorgi, G., Ferrini, B. S., Lo Porto, C., Lazzati, Z., Cocchi, D., Bruno, F., Greco, F., Riccio, A., and Bolzacchini, E.: Vertically-resolved particle size distribution within and above the mixing layer over the Milan metropolitan area, Atmos. Chem. Phys., 10, 3915-3932, doi:10.5194/acp-10-3915-2010, 2010.

Ferrero, L., Mocnik, G., Ferrini, B. S., Perrone, M. G., Sangiorgi, G., and Bolzacchini, E.: Vertical profiles of aerosol absorption coefficient from micro-aethalometer data and Mie calculation over Milan, Sci. Total Environ., 40, 2824-2837, doi:10.1016/j.scitotenv.2011.04.022, 2011a.

Ferrero, L., Riccio, A., Perrone, M. G., Sangiorgi, G., Ferrini, B. S., and Bolzacchini, E.: Mixing height determination by tethered balloon-based particle soundings and modeling simulations, Atmos. Res., 102, 145-156, doi:10.1016/j.atmosres.2011.06.016, 2011b.

Ferrero, L., Castelli, M., Ferrini, B. S., Moscatelli, M., Perrone, M. G., Sangiorgi, G., D'Angelo, L., Rovelli, G., Moroni, B., Scardazza, F., Mocnik, G., Bolzacchini, E., Petitta, M., and Cappelletti, D.: Impact of black carbon aerosol over Italian basin valleys: high-resolution measurements along vertical profiles, radiative forcing and heating rate, Atmos. Chem. Phys., 14, 9641-9664, doi:10.5194/acp-14-9641-2014, 2014.

Hagler, G. S. W., Yelverton, T. L. B., Vedantham, R., Hansen, A. D. A. and Turner, J. R.: Post-Processing Method to Reduce Noise while Preserving High Time Resolution in Aethalometer Real-Time Black Carbon Data, Aerosol Air Qual. Res., 11, 539-546, doi:10.4209/aaqr.2011.05.0055, 2011.

Hansen, A. D. A., Rosen, H., and Novakov, T.: The aethalometer - an instrument for the real-time measurement of optical absorption by aerosol particles, Sci. Total Environ., 36, 191-196, 1984.

Höpner, F., Bender, F. A. M., Ekman, A. M. L., Praveen, P. S., Bosch, C., Ogren, J. A., Andersson, A., Gustafsson, Ö. And Ramanathan, V.: Vertical profiles of optical and microphysical particle properties above the northern Indian Ocean during CARDEX 2012, Atmos. Chem. Phys., 16, 1045-1064, doi:10.5194/acp-16-1045-2016, 2016.

Hyvärinen, A. P., Vakkari, V., Laakso, L., Hooda, R. K., Sharma, V. P., Panwar, T. S., Beukes, J. P., van Zyl, P. G., Josipovic, M., Garland, R. M., Andreae, M. O., Pöschl, U., and Petzold, A.: Correction for a measurement artifact of the Multi-Angle Absorption Photometer (MAAP) at high black carbon mass concentration levels, Atmos. Meas. Tech., 6, 81-90, doi:10.5194/amt-6-81-2013, 2013.

IPCC: Summary for policymakers. Climate change 2013: the physical science basis, Cambridge University Press, Cambridge, UK and New York, NY, USA, 2216 pp, 2013.

Jacobson, M. Z.: Strong radiative heating due to the mixing state of black carbon in atmospheric aerosols, Nature, 409, 695-697, 2001.

Janssen, N. A., Gerlofs-Nijland, M. E., Lanki, T., Salonen, R. O., Cassee, F., Hoek, G., Fischer, P., Brunekreef, B., and Krzyzanowski, M.: Health effects of black carbon, World Health Organization, Copenhagen, 2012.

Kaimal, J. C., and Finnigan, J. J.: Atmospheric boundary layer flows: their structure and measurement, Oxford University Press, New York, 289 pp., 1994.

Kim, S. W., Yoon, S. C., Won, J. G., and Choi, S. C.: Ground-based remote sensing measurements of aerosol and ozone in an urban area: a case study of mixing height evolution and its effect on ground-level ozone concentrations, Atmos. Environ., 41, 7069-7081, doi:10.1016/j.atmosenv.2007.04.063, 2007.

Lazaridis, M.: First principles of meteorology and air pollution, Environ. Poll., Springer Netherlands, 362 pp., 2010.

Levy, R., and Hsu, C.: MODIS Atmosphere L2 Aerosol Product, NASA MODIS Adaptive Processing System, Goddard Space Flight Center, USA, http://dx.doi.org/10.5067/MODIS/MOD04_L2.006, and http://dx.doi.org/10.5067/MODIS/MYD04_L2.006, 2015.

Li, J., Fu, Q. Y., Huo, J. T., Wang, D. F., Yang, W., Bian, Q. G., Duan, Y. S., Zhang, Y. H., Pan, J., Lin, Y. F., Huang, K., Bai, Z. P., Wang, S. H., Fu, J. S., and Louie, P. K. K.: Tethered balloon-based black carbon profiles within the lower troposphere of Shanghai in the 2013 East China smog, Atmos. Environ., 123, 327-338, doi:10.1016/j.atmosenv.2015.08.096, 2015.

Liao, H., and Shang, J. J.: Regional warming by black carbon and tropospheric ozone: a review of progresses and research challenges in China, J. Meteor. Res., 29, 525-545, doi:10.1007/s13351-015-4120-0, 2015.

Ma, N., Zhao, C. S., Nowak, A., Müller, T., Pfeifer, S., Cheng, Y. F., Deng, Z.Z., Liu, P. F., Xu, W. Y., Ran, L., Yan, P., Göbel, T., Hallbauer, E., Mildenberger, K., Henning, S., Yu, J., Chen, L. L., Zhou, X. J., Stratmann, F., and Wiedensohler, A.: Aerosol optical properties in the North China Plain during HaChi campaign: an in-situ optical closure study, Atmos. Chem. Phys., 11, 5959-5973, doi:10.5194/acp-11-5959-2011, 2011.

Menon, S., Hansen, J., Nazarenko, L., Luo, Y. F.: Climate effects of black carbon aerosols in China and India, Science, 297, doi:10.1126/science.1075159, 2250-2253, 2002.

Metcalf, A. R., Craven, J. S., Ensberg, J. J., Brioude, J., Angevine, W., Sorooshian, A., Duong, H. T., Jonsson, H. H., Flagan, R. C., Seinfeld, J. H.: Black carbon aerosol over the Los Angeles Basin during CalNex, J. Geophys. Res., 117, D00V13, doi:10.1029/2011JD017255, 2012.

Miffre, A., Anselmo, C., Geffroy, S., Frejafon, E., and Rairoux, P.: Lidar remote sensing of laser-induced incandescence on light absorbing particles in the atmosphere, Opt. Exp., 23, 2347-2360, doi:10.1364/OE.23.002347, 2015.

Moosmüller, H., Chakrabarty, R. K., and Arnott, W. P.: Aerosol light absorption and its measurement: a review, J. Quant. Spectrosc. Radiat. Transfer, 110, 844-878, doi:10.1016/j.jqsrt.2009.02.035, 2009.

Müller, T., Henzing, J. S., de Leeuw, G., Wiedensohler, A., Alastuey, A., Angelov, H., Bizjak, M., Collaud Coen, M., Engström, J. E., Gruening, C., Hillamo, R., Hoffer, A., Imre, K., Ivanow, P., Jennings, G, Sun, J. Y., Kalivitis, N., Karlsson, H., Komppula, M., Laj, P., Li, S. M., Lunder, C., Marinoni, A., Martins dos Santos, S., Moerman, M., Nowak, A., Ogren, J. A., Petzold, A., Pichon, J. M., Rodriquez, S., Sharma, S., Sheridan, P. J., Teinilä, K., Tuch, T., Viana, M., Virkkula, A., Weingartner, E., Wilhelm, R., and Wang, Y. Q.: Characterization and intercomparison of aerosol absorption photometers: result of two intercomparison workshops, Atmos. Meas. Tech., 4, 245-268, doi:10.5194/amt-4-245-2011, 2011.

Nichols, J. L., Owens, E. O., Dutton, S. J., and Luben, T. J.: Systematic review of the effects of black carbon on cardiovascular, Int. J. Public Health, 58, 707-724, doi:10.1007/s00038-013-0492-z, 2013.

Petzold, A., and Schönlinner, M.: Multi-angle absorption photometry - a new method for the measurement of aerosol light absorption and atmospheric black carbon, J. Aerosol Sci., 35, 421-441, doi:10.1016/j.jaerosci.2003.09.005, 2004.

Petzold, A., Schloesser, H., Sheridan, P. J., Arnott, W. P., Ogren, J. A., and Virkkula, A.: Evaluation of multiangle absorption photometry for measuring aerosol light absorption, Aerosol Sci. Technol., 39, 40-51, doi: 10.1080/027868290901945, 2005.

Poulos, G. S., Blumen, W., Fritts, D. C., Lundquist, J. K., Sun, J. L., Burns, S. P., Nappo, C., Banta, R., Newsom, R., Cuxart, J., Terrandellas, E., Balsley, B., and Jensen, M.: CASES-99: a comprehensive investigation of the stable nocturnal boundary layer, Bull. Am. Meteorol. Soc., 83, 555-581, 2002.

Ramachandran, S., and Rajesh, T. A.: Black carbon aerosol mass concentrations over Ahmedabad, an urban location in western India: comparison with urban sites in Asia, Europe, Canada, and the United States, J. Geophys. Res., 112, D06211, doi:10.1029/2006JD007488, 2007.

Ramanathan, V., Chung, C., Kim, D., Bettge, T., Buja, L., Kiehl, J. T., Washington, W. M., Fu, Q., Sikka, D. R., and Wild, M.: Atmospheric brown clouds: impacts on South Asian climate and hydrological cycle, P. Nantl. Acad. Sci. USA, 102, 5326-5333, doi:10.1073/pnas.0500656102, 2005.

Ramanathan, V., and Carmichael, G.: Global and regional climate changes due to black carbon, Nature Geosci., 1, 221-227, 2008.

Ran, L., Deng, Z. Z., Wang, P. C., and Xia, X. A.: Black carbon and wavelength-dependent aerosol absorption in the North China Plain based on two-year aethalometer measurements, Atmos. Environ., 142, 132-144,

doi:10.1016/j.atmosenv.2016.07.014, 2016.

Ryerson, T. B., Andrews, A. E., Angevine, W. M., Bates, T. S., Brock, C. A., Cairns, B., Cohen, R. C., Cooper, O. R., de Gouw, J. A., Fehsenfeld, F. C., Ferrare, R. A., Fischer, M. L., Flagan, R. C., Goldstein, A. H., Hair, J. W., Hardesty, R. M., Hostetler, C. A., Jimenez, J. L., Langford, A. O., McCauley, E., McKeen, S. A., Molina, L. T., Nenes, A., Oltmans, S. J., Parrish, D. D., Pederson, J. R., Pierce, R. B., Prather, K., Quinn, P. K., Seinfeld, J. H., Senff, C. J., Sorooshian, A., Stutz, J., Surratt, J. D., Trainer, M., Volkamer, R., Williams, E. J., and Wofsy, S. C.: The 2010 California Research at the Nexus of Air Quality and Climate Change (CalNex) field study, J. Geophys. Res., 118, 5830-5866, doi:10.1002/jgrd.50331, 2013.

Safai, P. D., Raju, M. P., Maheshkumar, R. S., Kulkarni, J. R., Rao, P. S. P., and Devara, P. C. S.: Vertical profiles of black carbon aerosols over the urban locations in South India, Sci. Total Environ., 431, 323-331, doi:10.1016/j.scitotenv.2012.05.058, 2012.

Samset, B. H., Myhre, G., Schulz, M., Balkanski, Y., Bauer, S., Berntsen, T. K., Bian, H., Bellouin, N., Diehl, T., Easter, R. C., Ghan, S. J., Iversen, T., Kinne, S., Kirkevåg, A., Lamarque, J. F., Lin, G., Liu, X., Penner, J. E., Seland, Ø., Skeie, R. B., Stier, P., Takemura, T., Tsigaridis, K., and Zhang, K.: Black carbon vertical profiles strongly affect its radiative forcing uncertainty, Atmos. Chem. Phys., 13, 2423-2434, doi:10.5194/acp-13-2423-2013, 2013.

Sandradewi, J., Prevot, A. S. H., Weingartner, E., Schmidhauser, R., Gysel, M., and Baltensperger, U.: A study of wood burning and traffic aerosols in an Alpine valley using a multi-wavelength aethalometer, Atmos. Environ., 42, 101-112, doi:10.1016/j.atmosenv.2007.09.034, 2008.

Schmid, O., Artaxo, P., Arnott,W. P., Chand, D., Gatti, L. V., Frank, G. P., Hoffer, A., Schnaiter, M., and Andreae, M. O.: Spectral light absorption by ambient aerosols influenced by biomass burning in the Amazon Basin. I: comparison and field calibration of absorption measurement techniques, Atmos. Chem. Phys., 6, 3443-3462, doi:10.5194/acp-6-3443-2006, 2006.

Seibert, P., Beyrich, F., Gryning, S. E., Joffre, S., Rasmussen, A., and Tercier, P.: Review and intercomparison of operational methods for the determination of the mixing height, Atmos. Environ., 34. 1001-1027, doi:10.1016/S1352-2310(99)00349-0, 2000.

Shao, M., Tang, X. Y., Zhang, Y. H., and Li, W. J.: City clusters in China: air and surface water pollution, Front. Ecol. Environ., 4, 353-361, doi:10.1890/1540-9295(2006)004[0353:CCICAA]2.0.CO;2, 2006.

Stier, P., Seinfeld, J. H., Kinne, S., and Boucher, O.: Aerosol absorption and radiative forcing, Atmos. Chem. Phys., 7, 5237-5261, doi:10.5194/acp-7-5237-2007, 2007.

Streets, D. G., Gupta, S., Waldhoff, S. T., Wang, M. Q., Bond, T. C., and Bo, Y. Y.: Black carbon emissions in China, Atmos. Environ., 35, 4281-4296, doi:10.1016/S1352-2310(01)00179-0, 2001.

Tripathi, S. N., Dey, S., Satheesh, S. K., Lal, S., and Venkataramani, S.: Enhanced layer of black carbon in a north Indian

删除的内容: submitted,

industrial Indian city, Geophys. Res. Lett., 32, L12802, doi:10.1029/2005GL022564, 2005.

Tripathi, S. N., Srivastava, A. K., Dey, S., Satheesh, S. K., Krishnamoorthy, K.: The vertical profile off atmospheric heating rate of black carbon aerosols at Kanpur in northern India, Atmos. Environ., 41, 6909-6915, doi:10.1016/j.atmosenv.2007.06.032, 2007.

Virkkula, A., Mäkelä, T., Hillamo, R., Yli-Tuomi, T., Hirsikko, A., Hämeri, K., and Koponen, I. K.: A simple procedure for correcting loading effects of aethalometer data, J. Air Waste Manage. Assoc, 57, 1214-1222, doi:10.3155/1047-3289.57.10.1214, 2007.

Weingartner, E., Saathoff, H., Schnaiter, M., Streit, N., Bitnar, B., and Baltensperger, U.: Absorption of light by soot particles: determination of the absorption coefficient by means of aethalometers, J. Aerosol Sci., 34, 1445-1463, doi:10.1016/S0021-8502(03)00359-8, 2003.

Xu, W. Y., Zhao, C. S., Ran, L., Deng, Z. Z., Liu, P. F., Ma, N., Lin, W. L., Xu, X. B., Yan, P., He, X., Yu, J., Liang, W. D., and Chen, L. L.: Characteristics of pollutants and their correlation to meteorological conditions at a suburban site in the North China Plain, Atmos. Chem. Phys., 11, 4353-4369, doi:10.5194/acp-11-4353-2011, 2011.

Yu, T. W.: Determining height of the nocturnal boundary layer, J. Appl. Meteorol., 17, 28-33, 1978.

Yu, H. B., Liu, S. C., and Dickinson, R. E.: Radiative effects of aerosols on the evolution of the atmospheric boundary layer, J. Geophys. Res., 107, D12, doi:4142, 10.1029/2001JD000754, 2002.

Zarzycki, C. M. and Bond, T. C.: How much can the vertical distribution of black carbon affect its global direct radiative forcing?, Geophys. Res. Lett., 37, L20807, doi:10.1029/2010gl044555, 2010.

Zhao, D. L., Tie, X. X., Gao, Y., Zhang, Q., Tan, H. J., Bi, K., Jin, Y. L., and Chen, P. F.: In-situ aircraft measurements of the vertical distribution of black carbon in the lower troposphere of beijing, china, in the Spring and Summer Time, Atmos., 6, 713-731; doi:10.3390/atmos6050713, 2015.

Zhang, D. Z., Chen, B., Yamada, M., Niu, H. Y., Wang, B., Iwasaka, Y., and Shi, G. Y.: Elevated soot layer in polluted urban atmosphere: a case study in Beijing, J. Meteorol. Soc. Japan, 90, 361-375, doi:10.2151/jmsj.2012-302, 2012.

Zhang, X., Tang, J., Wu, Y. F., Wu, J., Yan, P., and Zhang, R. J.: Variations of black carbon aerosol observed in Beijing and surrounding area during 2006-2012, China Powder Sci. Tech., 21, 24-35, doi:10.13732/j.issn.1008-5548.2015.04.006, 2015.

删除的内容: L

Table 1 A statistical summary of the field campaign and the meteorology. H_{max} denotes the maximum height reached by the tethered balloon. T_{10m}, RH_{10m}, and WS_{10m} indicated temperature, relative humidity, and wind speed within 10 m near the surface, in the form of average value±standard deviation. WD_{10m} represents frequently encountered wind direction. The last column gives the weather that mostly occurred during each period.

Periods	Profiles	H_{max} (km)	T_{10m} (°C)	RH_{10m} (%)	WS_{10m} (m s^{-1})	WD_{10m}	Weather
06:00-09:00	23	0.28~0.92	25.3±0.8	62.7±3.2	2.9±1.3	Southwest	Cloudy
09:00-12:00	20	0.32~1.06	26.0±1.5	61.0±3.4	2.6±1.1	Southwest	Cloudy
12:00-15:00	4	0.84~1.14	28.7±2.3	55.9±5.0	2.2±1.4	Southeast	Fine
15:00-18:00	6	1.04~1.08	28.5±2.4	58.7±4.6	2.1±1.1	Southeast	Fine
18:00-21:00	14	0.26~1.16	29.1±2.2	45.0±3.3	1.8±0.8	Southwest	Fine

Table 2 Statistical parameters for BC vertical profiles measured during different periods. Notations for the parameters have been given in the text.

Parameters	06:00-09:00 23 Profiles	09:00-12:00 20 Profiles	12:00-15:00 4 Profiles	15:00-18:00 6 Profiles	18:00-21:00 14 Profiles
H_m (km)	0.08~0.29	0.18~0.87	0.43~1.14	0.69~1.08	0.19~0.25
H_e (km)	0.05±0.04	0.05±0.03			
C_m (μg m^{-3})	3.1~14.49 (6.61±2.93)	2.56~5.80 (4.42±1.11)	1.12~6.15 (3.77±2.06)	2.04~4.11 (3.05±0.86)	
C_f (μg m^{-3})	0.46~3.14 (1.67±0.95)	0.41~2.51 (1. 77±0.75)			0.36~2.83 (1.36±1.12)

Table 3 Measurements of BC vertical distributions in different regions. m_{BC} is the range and/or average value±standard deviation of BC mass concentrations, depending upon what is available in the literature. Height specifies how m_{BC} is obtained.

Locations	Type	Period	Method	m_{BC} (μg m^{-3})	Height	References
Los Angeles Basin, USA	Mixture	May 2010	Aircraft, SP2*	0.01~0.53	0.3 km	Metcalf et al., 2012
				0.03±0.05	FT	
Milan, Italy	Urban	Feb. 2010	Tethered balloon, AE-51	7.57 ± 1.28	ML	Ferrero et al., 2014
				2.03 ± 0.34	FT	
Multi-cities, India	Urban	Jun. 2005	Aircraft, AE-42, AE-21	1.50~7.50	PBL	Safai et al., 2012 and references therein
Beijing, China	Urban	May-Jun. 2012	Aircraft, SP2	0.24~4.02	PBL	Zhao et al., 2015
Shanghai, China	Urban	Dec. 2013	Tethered balloon, AE-31	3.20~7.30	0-1 km	Li et al., 2015
Central NCP, China	Semirural	Jun.-Jul. 2014	Tethered balloon, AE-51	1.12~14.49	ML	This study
				(5.16±2.49)		
				0.36~3.14	FT	
				(1.61±0.94)		

* SP2: Single Particle Soot Photometer

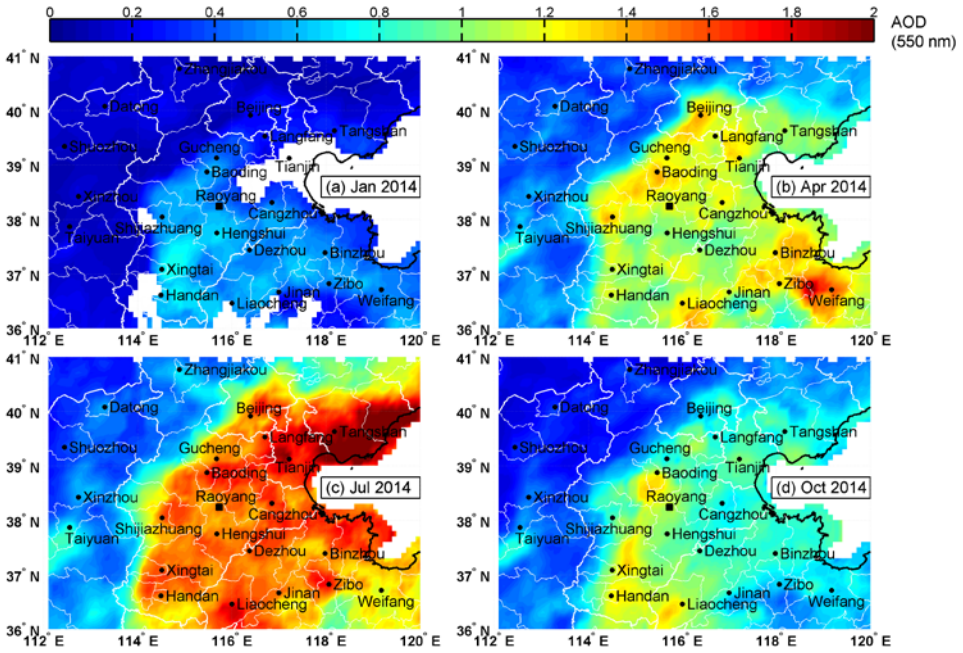

Figure 1. The spatial distribution of averaged MODIS aerosol optical depth (AOD) at 550 nm in (a) January; (b) April; (c) July; (d) October, 2014 in the NCP. The locations of the semirural site Raoyang and major cities are respectively marked by square and dots. Only grids with the fraction of valid data exceeding 30% in the month are shown.

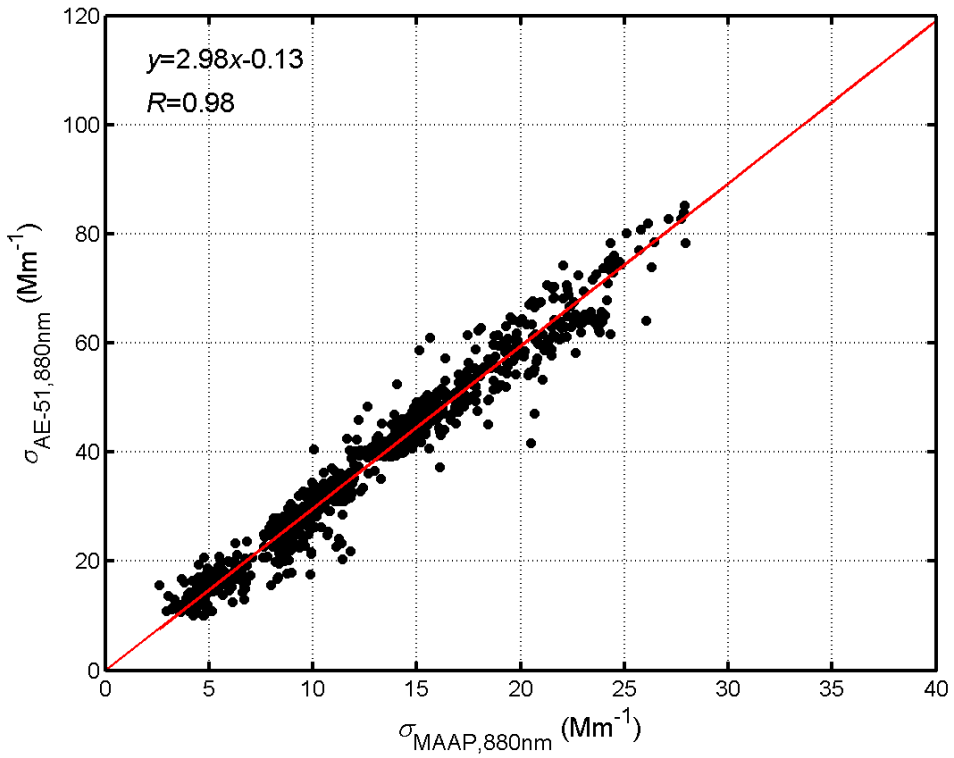

Figure 2. Reduced major axis regression of attenuation coefficients $\sigma_{AE\text{-}51,880}$ (ATN<10) measured by AE-51 and absorption coefficients σ_{880nm} calculated from concomitant MAAP and AE-31 measurements in the comparative test.

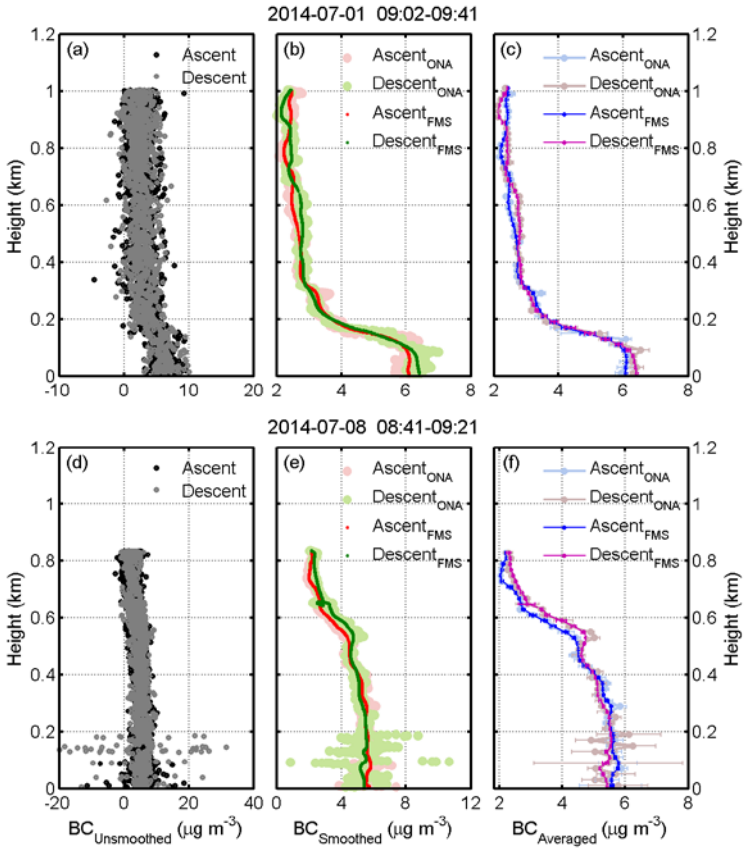

Figure 3. (a) Unsmoothed BC mass concentrations measured with a temporal resolution of 1 s on July 1, 2014 (09:02-09:41 LT). Data points collected from the ascending and descending process are respectively marked in black and grey dots. (b) Smoothed BC mass concentrations using two algorithms. Data points processed by the ONA method are displayed in large pink dots for the ascent and in light green color for the descent. Data points processed by the FMS method are denoted by small red dots for the ascent and green dots for the descent. (c) 20-m averaged profiles based upon smoothed data using two algorithms. Dots indicate 20-m averages, with standard deviations in error bars. Results from the ONA and FMS methods are respectively given in the color of light blue and blue for the ascent, while in the color of light purple and purple for the descent. (d)-(f) Measured and processed BC vertical profiles on July 8, 2014 (08:41-09:21 LT). The caption is the same as that in (a)-(c).

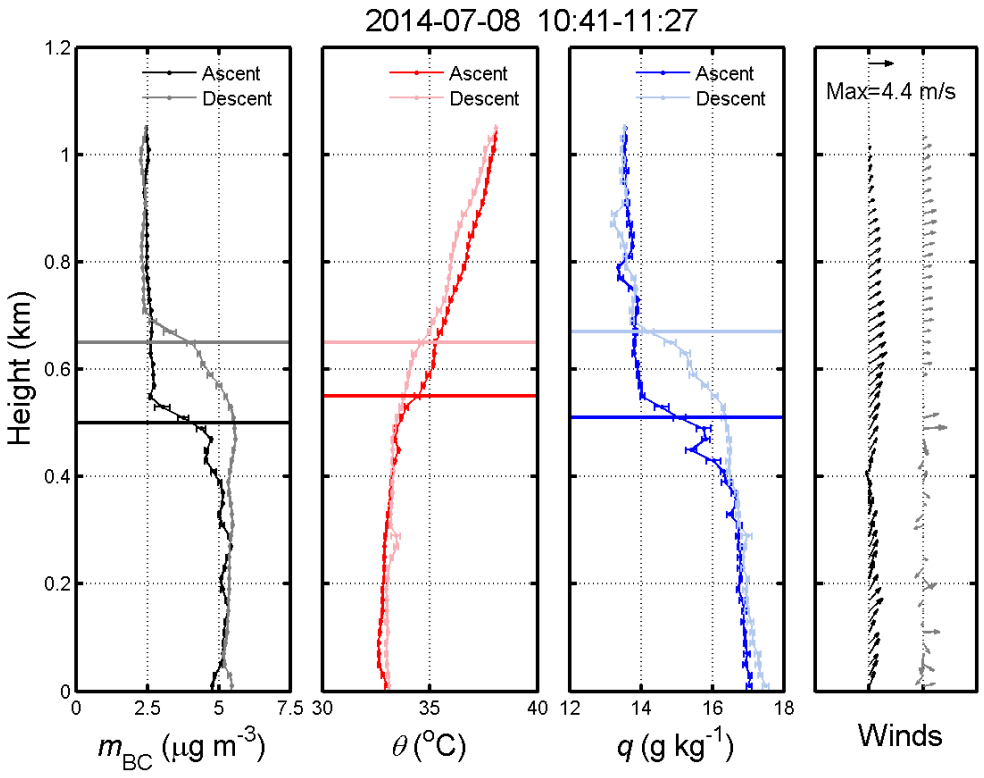

Figure 4. Vertical profiles of BC mass concentrations (m_{BC}), potential temperature (θ), specific humidity (q) and winds on July 8, 2014 (10:41-11:27 LT). Profiles measured during the ascent are displayed in dark colors, while the descent in light colors. Dots indicate 20-m averaged data, with standard deviations in error bars. Heights of the mixing layer (ML) estimated from vertical profiles are given in horizontal lines. Arrows show vector mean horizontal winds, with northerly winds indicated by downward arrows. The wind vector for the maximum wind speed is marked with the text.

删除的内容: 1

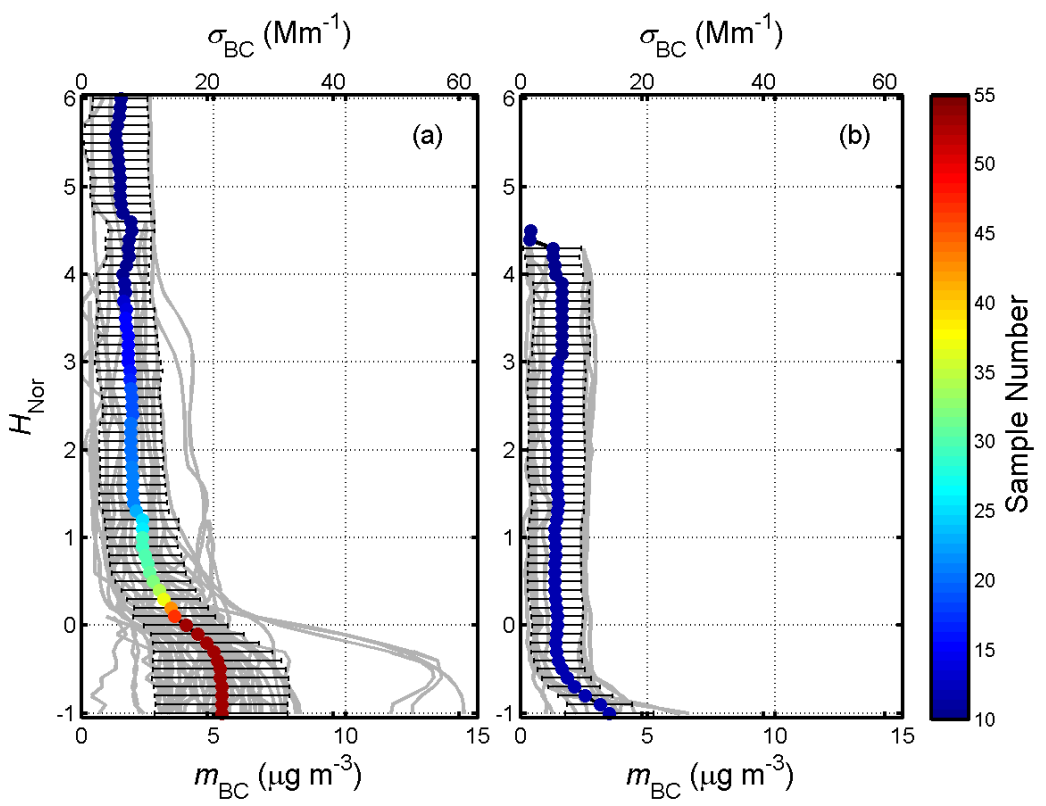

Figure 5. Vertical distributions of m_{BC} (bottom axis) and σ_{BC} (top axis) along the normalized height H_{Nor} (a) in the daytime and (b) in the evening during the field campaign (grey lines). The average profile is shown in black line, with error bars to represent standard deviations. Average values are indicated by dots, with the color to show the number of samples at each layer.

删除的内容:

删除的内容: 2

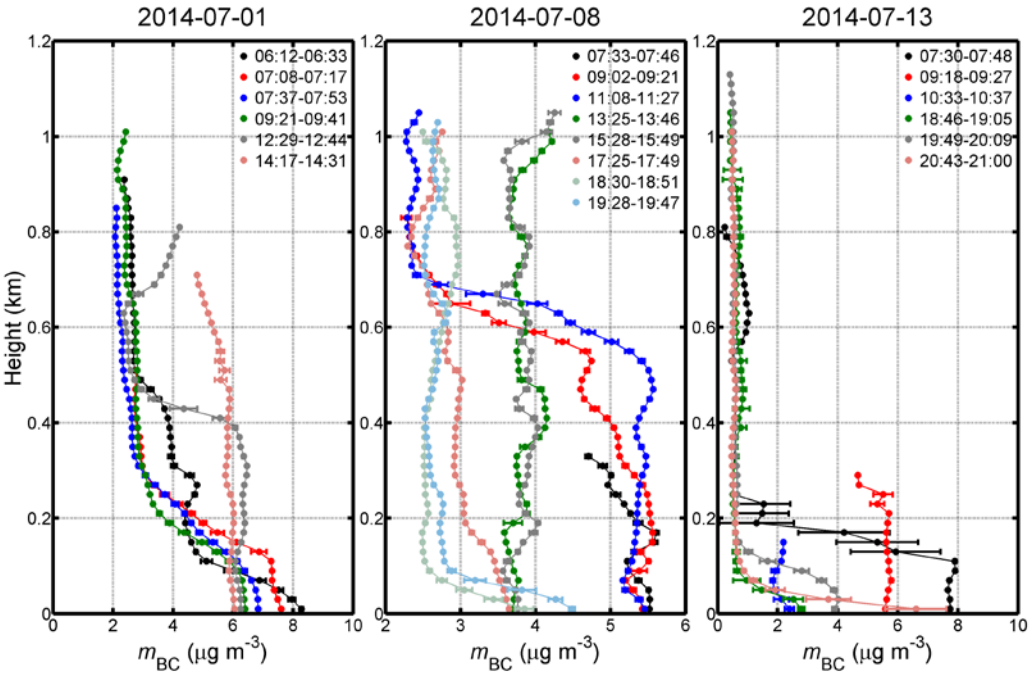

Figure 6. Vertical distributions of BC separately displayed for July 1, 8, and 13. Profiles collected at different time are shown in different colors. As in Fig. 4, dots represent 20-m averaged m_{BC}, with standard deviations given in error bars.

删除的内容: 3

删除的内容: 1

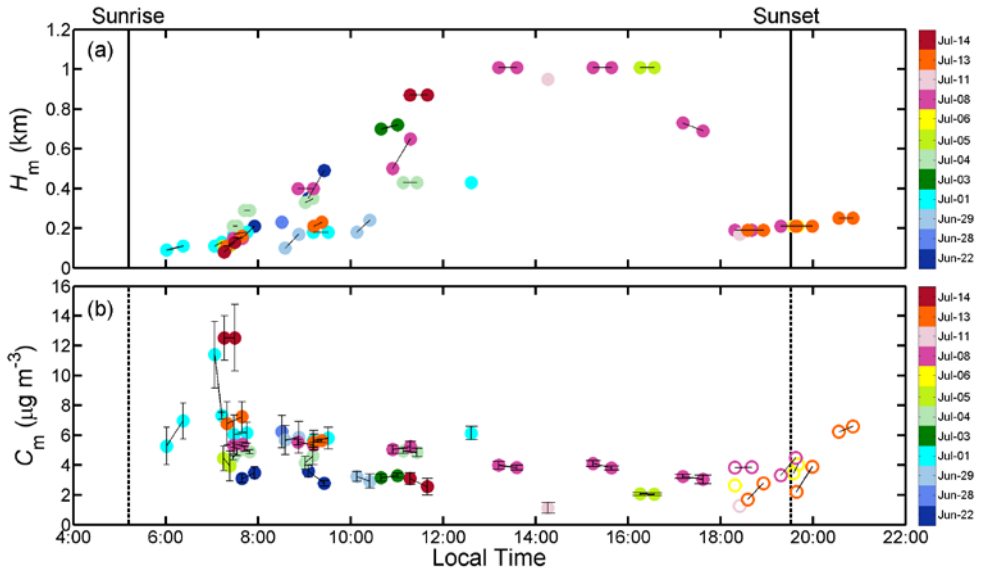

Figure 7. (a) H_m identified from BC vertical profiles in the selected dataset. Measurements made on different days are marked by dots in different colors. H_m from the ascent and descent of one launch are connected by black lines. (b) Average m_{BC} within the ML (C_m) during the daytime (before 18:00 LT) are marked by solid dots. Average m_{BC} within 20 m near the surface in the evening are marked by open dots.

删除的内容: 4